Towards 3D Bioprinting of a Vascularized Convoluted Proximal Tubule

Towards 3D Bioprinting of a Vascularized Convoluted Proximal Tubule

Jessica E. Herrmann
A.B. Degree Candidate in Biomedical Engineering

A senior research thesis submitted in partial fulfillment of the degree of Bachelor of Arts in Biomedical Engineering at Harvard University

Faculty Adviser: Dr. Jennifer A. Lewis

Harvard John A. Paulson School of Engineering and Applied Sciences
Cambridge, MA

March 31, 2017

Table of Contents

Abstract 1

I. Introduction 2

II. Materials 8

Cellular Culture 8

Cell Lines 8

Culture Protocols 8

Biomaterials 9

Extracellular Matrix 9

Biocompatible Ink 9

Chip Materials 10

Perfusion System 10

Polydimethylsiloxane Ink 11

III. Methods 12

Chip Construction and Maintenance 12

Cellular Culture 12

Generation of G-Code for the 3D Printers 12

Chip Construction and Assembly 12

Cell Seeding of the Bioprinted Channels 14

Pin Pullout Technique to Generate Channels 14

MTS Assay 15

Graphical and Statistical Analysis 15

Setup and Culturing Conditions 16

MTS Assays for HUVEC-Tert and PTEC-Tert Compatibility 16

MTS Assays for RFP-GMEC and PTEC-Tert Compatibility 17

MTS Assays for PTEC-Tert, Primary PTEC, and RFP-GMEC Compatibility 17

Immunostaining and Imaging 18

Immunostaining Static 2D Samples 18

Immunostaining 3D-Perfused Chips 19
Confocal Imaging and Analysis 20
PTEC-Tert and RFP-GMEC Morphology and Expression in 2D Static Culture 20
PTEC-Tert and RFP-GMEC Morphology and Expression in 3D-Perfused Culture 20
Locked-Nucleic Acid Transport Assay 21
IV. Results 22
Design of the Vascularized Model of the Convoluted Proximal Tubule 22
Developing the Model 22
Selection of the Renal and Vascular Cell Lines 23
HUVEC-Terts in 3D-Perfused Co-Culture with PTEC-Terts 23
PTEC-Tert Media Lowers Viability of HUVEC-Terts 24
Antagonism of HUVEC-Terts by PTEC-Tert Media is Unidirectional 26
RFP-GMECs Exhibit Enhanced Tolerance of PTEC-Tert Media Relative to HUVEC-Terts 27
PTEC-Terts and Primary PTECs Yield Comparable Viabilities 29
Characterizing Cellular Morphology and Expression on the Extracellular Matrix 29
RFP-GMECs and PTEC-Terts Show Characteristic Morphology on ECMs in 2D Culture 30
RFP-GMECs Express Appropriate Vascular Markers in 3D-Perfused Culture 32
PTEC-Terts Express Appropriate Renal Markers in 3D-Perfused Culture 33
Assessing Transepithelial Transport 36
PTEC-Terts Exhibit Transepithelial Transport of Locked-Nucleic Acid 36
Seeding the Vascularized Proximal Tubule Model 38
PTEC-Terts and RFP-GMECs Survive for Three Weeks in 3D-Perfused Co-Culture 38
V. Discussion 39
VI. Conclusion 45
VII. Supplementary Information 46
Analyzing the Role of Curvature Within the Convoluted Proximal Tubule 46
Minimizing the Diameter of the Proximal Tubule: Pin Pullout Using Glass Capillaries 47
VIII. Acknowledgments 50
IX. References 51

Abstract

Three-dimensional (3D) constructs that recapitulate native tissue architectures offer biomimetic microenvironments in which to perform improved pharmacological studies of drug efficacy and toxicity. The convoluted proximal tubule (PT) is the principal site implicated in renal disease progression and presents an ideal target for disease modeling and therapeutics. Although previous investigators have developed 3D structures that reproduce specific proximal tubule morphologies and functions, these models have been limited by their lack of integrated vasculature to simulate crucial reabsorption and transport processes between the proximal tubule and adjoining blood vessels. This thesis sought to expand the functionality of current proximal-tubule-on-chip technologies by 3D bioprinting a vascularized PT. The model explored in this thesis incorporated cellular compatibilities, extracellular matrix formulations, and geometric design considerations to demonstrate co-culture of adjacent endothelialized and epithelialized tubules for three weeks under 3D-perfused flow. The MTS cell proliferation assay was utilized to select glomerular microvascular endothelial cells expressing red fluorescent protein (RFP-GMECs) as the vascular cell line for 3D perfused co-culture with immortalized proximal tubule epithelial cells (PTECs-Terts). The RFP-GMECs and PTEC-Terts expressed appropriate vascular and renal cell markers when cultured on extracellular matrices statically and under flow. Transepithelial transport of locked-nucleic acid across the proximal tubule channel lining was further demonstrated in a non-endothelialized model. Ultimately, RFP-GMECs and PTEC-Terts were successfully co-cultured in a vascularized PT model for three weeks. The vascularized PT construct presented here enables functional assays of active transport processes, analysis of nephrotoxic drug effects, and exploration of altered tubular architectures. Various biological and technical considerations can be individually addressed through this customizable 3D model, permitting analysis of engineering principles essential to developing more complicated versions of the vascularized proximal tubule and, ultimately, larger scale renal tissue.

I. Introduction

In recent years, widespread medical and pharmacological need has escalated the desire to manufacture renal tissue. Renal damage can be drug-induced or biologically developed in response to natural or synthetic sources, and primarily presents as Acute Kidney Injury (AKI) or Chronic Kidney Disease (CKD) [1]. AKI is a provisional condition characterized by temporary loss of kidney function with potential long-term consequences, while CKD encompasses long-term renal failure. According to a report published by the 2016 United States Renal Data System, the prevalence of CKD in the United States has increased from approximately 12% in 1988 to 14.8% in 2014 [2]. Various medications are often prescribed to manage AKI and CKD symptoms and their related physiological issues, including mineral and water homeostasis, which are necessary to maintain vital kidney function. In advanced cases, patients may require dialysis or renal transplantation to replace these vital functions. These treatments may be invasive, are often expensive, and may be simply inaccessible based on organ donor availability. From a medical standpoint, implantable renal tissue or improved renal drug testing environments offer an opportunity to research renal injuries, study repair mechanisms, and develop more effective treatment options.

Since the kidney is a structurally complex organ comprised of multiple tissues with specialized functions, it contains numerous targets for arresting disease progression [3]. Many of these sites occur within the nephron, the fundamental unit of the kidney that includes the glomerulus and an attached tubular pathway along which reabsorption and re-filtration of the renal filtrate occur. In particular, the convoluted proximal tubule (PT) and its associated glomerulotubular junction present vulnerable structures within the nephron for induced renal injury [4, 5]. The PT contributes over 50% of renal volume and has a tubular length of approximately 12 mm at full maturity [4]. Damage to the proximal tubule, as occurs in the disorder nephropathic cystinosis, has been linked to CKD progression. [4]. The convoluted PT therefore offers one of the most promising pharmaceutical targets for the prevention and treatment of renal disease.

Engineered 3D proximal tubules offer significant potential to improve pharmacological studies of drug efficacy and toxicity. To effectively recapitulate physiological processes, engineered PT tissue environments must contain specific biomimetic features that promote structural and functional integrity. In particular, the extracellular matrix (ECM) represents an essential component of tissue that must be incorporated into engineered constructs. The ECM consists of the non-cellular components of tissue secreted locally by cells. Within all tissues, the ECM regulates cellular

adhesion, maturation, and behavior [6]. In addition to providing scaffolding for cellular structures, the ECM plays a central role in biological signaling and cellular metabolism through its specific binding sites and through the diffusional transport of proteins, waste products, and other molecules through its porous matrix. In human proximal tubule cells specifically, Zhang *et al.* demonstrated that ECM composition altered cellular growth and transport processes [6].

The extent to which the tissue mimics native 3D architectures further alters cellular response [7]. Recent insights into the limitations of static culturing dishes have led to the development of 3D culturing systems that possess numerous advantages over two-dimensional (2D) systems. From a structural standpoint, 3D systems enable greater incorporation of biomaterials to simulate crucial tissue features such as chemical composition and mechanical properties of the ECM, as well as compartmentalization for enhanced cellular heterogeneity [7, 8]. 3D systems further permit the introduction of sustained, automated fluid flow through tubular architectures [9]. Within tubes lined with proximal tubule epithelial cells (PTECs) or vascular cells, the resulting shear stresses can induce differential cellular responses that better replicate *in vivo* behaviors [10, 11]. Critically, it is not only the addition of the third dimension itself that accounts for altered cellular behavior, but rather, the additive combination of variations in mechanical and molecular components permitted by different dimensionalities [7]. Overall, 3D tissue microenvironments introduce greater accuracy into *in vitro* studies of nephrotoxicity than standard 2D culturing techniques by providing biomimetic features that enhance the prediction of *in vivo* cellular responses to drugs.

Elements of engineered tissue constructs interact closely with one another through dependent biological processes and must therefore operate synergistically to successfully reproduce biomimetic behaviors. Within the kidney, approaches to modeling the proximal tubule have focused on integrating these features to permit the reliable reproduction of physiological forces. Organ-on-chip microfluidic devices have presented significant promise for combining these elements to simulate the biological forces, chemical gradients, and physiological geometries that comprise tissue functionality. While multiple biological structures have been modeled, several laboratories have focused on proximal tubule-on-a-chip devices for investigating renal processes. Notably, Donald Ingber's laboratory at the Wyss Institute for Biologically Inspired Engineering has engineered such a system for analyzing nephrotoxicity and drug transport [12]. Their chip consists of two adjacent channels embedded within a polydimethylsiloxane (PDMS) core. A porous membrane coated in collagen type IV, an ECM protein, provides a separating interface between the channels to simulate cellular interactions across the ECM. The upper channel, which rests on top of the membrane,

contains primary human kidney proximal tubule epithelial cells (PTECs), while the acellular lower channel contains culture medium. The epithelialized channel is perfused with medium at a physiologically relevant shear stress of 0.2 dynes/cm^2 while the medium in the lower channel remains static to simulate the interstitial renal compartment and to act as a reservoir for collecting molecules transported across the epithelial barrier. The model exhibited enhanced cilia formation and PTEC polarization relative to 2D controls [12].

Despite its successful recapitulation of multiple proximal tubule functions, this microfluidic device was subject to numerous limitations. The epithelialized channel was not circumscribed by the extracellular matrix, but rather, exposed to it on only one side. This compromised the 3D nature of the construct and did not mimic physiological conditions, where the convoluted proximal tubule is embedded completely within the ECM. Additionally, the channels themselves were not tubular in shape. Since Sekiya *et al.* demonstrated that tubular arrangement of porcine renal proximal tubule cells altered surface marker expression relative to 2D monolayers [13], tubular architecture represents an important component of biomimetic PT recapitulation.

Nortis, a microfluidic organ-on-a-chip company that emerged from research conducted by Weber *et al.* at the University of Washington, has developed a 3D microphysiological system (MPS) that overcomes these limitations by embedding tubular channels with an extracellular matrix gel [14]. Their work demonstrated enhanced biomarker expression relative to the microfluidic device created by Jang *et al.* Additionally, Nortis performed functional assays to demonstrate increased transepithelial transport of organic solutes within their model relative to 2D controls and demonstrated healthy morphological features [14].

However, neither the work of Jang *et al.* nor of Weber *et al.* incorporate vascular lines for supplying the cells with nutrients [12, 14] or analyzing PT reuptake processes. The kidney is one of the most heavily vascularized organ systems in the body. Collectively, renal structures receive approximately 20% of cardiac output [2]. The vasculature performs functions essential to cellular health by transporting nutrients, oxygen, and waste products throughout the body in the form of circulating arterial blood. As arteries approach the kidney, they branch into narrow capillaries across whose membranes molecules can be exchanged. The molecules exit the capillaries, diffuse across the interstitial extracellular matrix, and enter cells via active or passive transport processes. Cells then utilize the nutrients and secrete waste products or signaling molecules into the bloodstream for delivery to other appropriate tissues or for removal from the body. Blood vessels are therefore necessary for renal filtration and reabsorption processes, as well as for directional transport.

Additionally, although not the focus of this thesis, vasculature could more broadly provide engineered tissue constructs with a native source of nutrients for enhanced cellular longevity. Incorporating vasculature into microfluidic devices simulating the proximal tubule represents a necessary step in extending their physiological functionality and biomimetic accuracy.

Several investigators have previously attempted to integrate vasculature into on-chip models of tubule structures. Mimetas, a company that focuses on organ-on-chip microfluidic technologies, has developed a microfluidic culturing plate that permits adjacent co-culture of independently perfusable tubules [15]. One of these tubules can be lined with vascular cells while the other contains epithelial cells. Their culturing system establishes the potential to perform nephrotoxicity assays and cellular transport studies without impeding membranes. However, their culturing system is restricted to microwell plates for drug screening assays, and cannot be scaled up to produce more complex tissue architectures. Additionally, their OrganoPlates® rely on physical "phaseguides" between the channels to pattern materials via capillary pressures. The phaseguides partially obstruct the tissue-tissue interface [15]. Finally, Mimetas establishes perfusion through specific rocking motions, and cannot interface with peristaltic pumps to achieve unidirectional, consistent flow.

The Lewis Laboratory seeks to address the technical and biological limitations of vascularized proximal tubule-on-a-chip systems through 3D bioprinting. 3D bioprinting enables direct writing of custom tubular geometries and encapsulation of the printed networks within an extracellular matrix. Numerous fugitive, polymeric, and elastomeric inks can be incorporated into this process. In particular, printing with acellular fugitive inks that are later evacuated from the surrounding extracellular matrix yields open lumens that one can subsequently seed with cells. The method further permits printing with cell-laden inks to directly form living architectures. 3D bioprinting offers significant advantages over alternative techniques for generating microfluidic devices. Notably, bioprinting permits high-throughput fabrication of readily adaptable tubular geometries. These structures are reproducible and can be made increasingly complex through layer-by-layer deposition of ink materials [8, 16]. Preexisting on-chip microfluidic models of the proximal tubule have not permitted such dynamic alteration of the system design. Although organ-on-chip company Organovo recently reported 3D bioprinted tubulointerstitial interfaces, their constructs were not perfusable and instead examined only the cellular-matrix interface. Critically, their model does not incorporate laminar flow to subject the epithelial cells to shear stresses, nor does it confine them to a 3D geometry [17]. The Lewis Laboratory has previously employed 3D bioprinting to

develop a heterogeneous, vascularized thick tissue construct that was sustained under flow for over six weeks in culture [8].

Most recently, our team bioprinted a perfusable, functional model of a convoluted proximal tubule embedded within a biocompatible extracellular matrix (figure 1a) [9]. The 3D PT model can be lined with epithelial cells and used to study cytotoxic drug effects, analyze cellular behavior, or perform characterizing assays. In particular, the PT demonstrated albumin uptake by PTECs within the perfused channel and cytotoxic response to the drug cyclosporin A, which has known nephrotoxic effects (figure 1b). The proximal tubule model further demonstrated enhanced morphological features relative to 2D controls, including elongated microvilli lengths and cell polarity [9]. Although our model represented the first 3D bioprinted perfusable proximal tubule, it similarly did not include an endothelialized vascular line, motivating the research behind this thesis to introduce a blood vessel into the system.

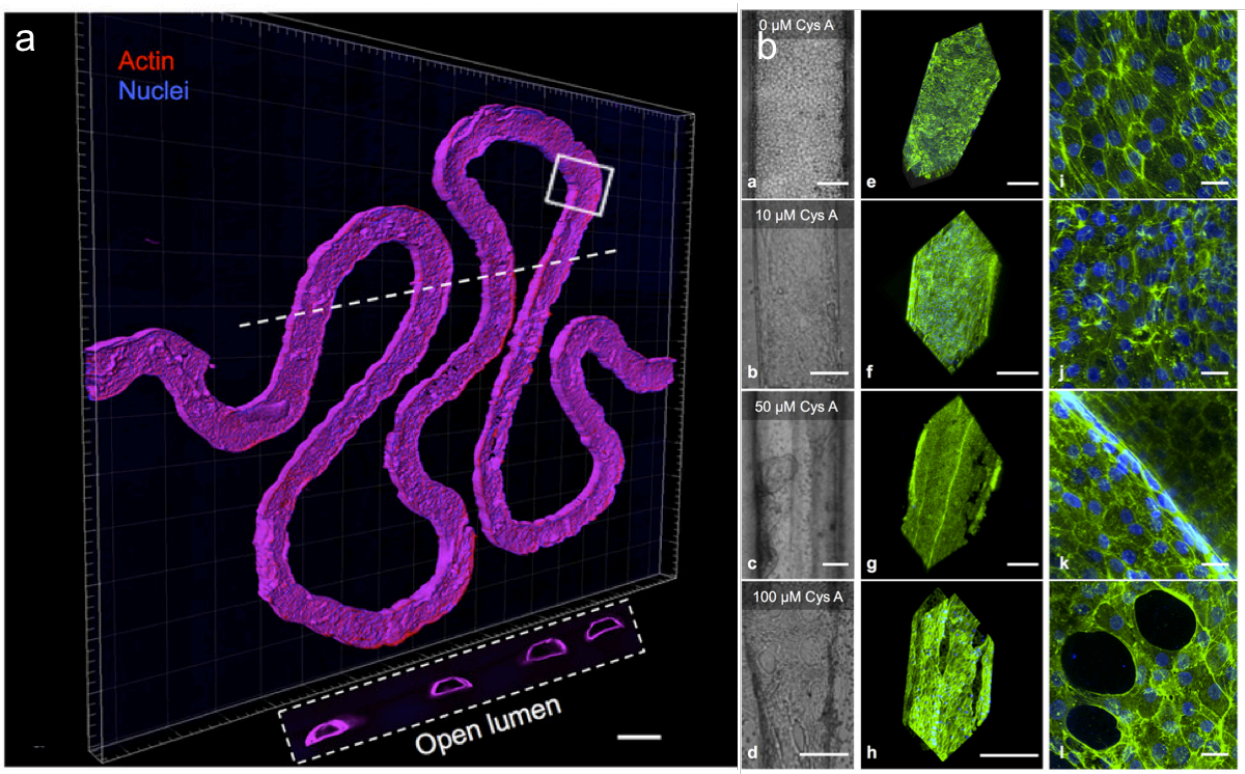

Figure 1: 3D bioprinted model of a convoluted renal proximal tubule and associated nephrotoxicity study. Figure (a) depicts the 3D bioprinted convoluted proximal tubule with a scale bar of 500 μm. Figure (b) demonstrates cytotoxic effects of increased cyclosporin A concentration on the proximal tubule epithelial cells, with actin stained in green and nuclei stained in blue. The scale bars correspond to 200 μm in (ba-h) and 20 μm in (bi-l). These images have been adapted from figure 1 and figure 5 of the work conducted by Homan *et al.* [9].

This thesis explores the biological and technical considerations inherent in bioprinting a vascularized, perfusable 3D model of the convoluted proximal tubule. In particular, the work examines cellular compatibilities between the renal and the vascular cell lines, impact of extracellular matrix formulations on cellular morphology, and transepithelial transport by PTECs within perfused culture, to ultimately demonstrate a preliminary 3D bioprinted system that embeds adjacent vascular and proximal tubule channels within an ECM. Taken together, this thesis presents the first functional step towards integrating vasculature into the 3D perfused proximal tubule model previously reported by the Lewis Laboratory.

II. Materials

Cellular Culture

Cell Lines

Cell lines utilized in experiments included immortalized human umbilical vein endothelial cells (HUVEC/TERT2, ATCC CRL-4053), immortalized human renal proximal tubule epithelial cells (RPTEC/TERT1, ATCC CRL-4031), primary human renal proximal tubule epithelial cells (ScienceCell), human glomerular microvascular endothelial cells expressing red fluorescent protein (Angio-Proteomie, ref. #cAP-0004RFP), and human glomerular microvascular endothelial cells not expressing fluorescent protein (Angio-Proteomie). This thesis refers to the cells as HUVEC-Terts, PTEC-Terts, primary PTECs, RFP-GMECs, and GMECs, respectively.

Culture Protocols

All cells were cultured in base, culture, or conditioned medium. Base medium consisted of a foundational media formulation, while culture medium consisted of the base medium with added growth factors and media supplements (referred to as "components" in subsequent sections). The supplements were also produced by ATCC and Lonza and were added to the base media according to protocols published by these companies. The PTEC-Tert base medium (ref. #CRL-4031) and the vascular cell basal medium for HUVEC-Terts (ref. #PCS-100-030) were both produced by ATCC. The RFP-GMECs and GMECs were cultured using the same media, which was produced by Lonza. The media was prepared by combining Lonza Endothelial Basal Media (EBM-2, ref. #CC-3156) with the EGM-2 SingleQuots pack (ref. #CC-3162). The primary PTEC medium was identical to the PTEC-Tert medium with the exception that it also contained 2% fetal bovine serum (FBS). When used to culture cells in 3D constructs via perfusion, all media additionally contained 1% aprotonin and 1% antibiotic-antimycotic.

To prepare the PTEC-Tert and primary PTEC media, 4.425 g of lyophilized DMEM F-12 without glucose (US Biological Life Sciences, Ref# D9807-02) were added to 500 mL of double-distilled water. The following supplemental media components, which were purchased from Sigma, included: sodium bicarbonate, dextrose, insulin-transferrin-selenium, triiodothyronine, sodium selenite, prostaglandin E1, hydrocortisone, geneticin, and ascorbic acid. Hydrochloric acid was used to titrate the pH to 7.3 before filter-sterilizing the medium using a 0.22 μm filter. After filtering, human recombinant epidermal growth factor produced by R&D Systems was added to the medium and the solution was stored at 4°C prior to use.

To prepare the HUVEC-Tert medium, the Vascular Cell Endothelial Growth Kit-VEGF (ATCC PCS-100-041) was added to the ATCC vascular cell basal medium. The growth kit contained: human recombinant vascular endothelial growth factor, human recombinant epidermal growth factor, human recombinant fibroblast growth factor, human recombinant insulin-like growth factor, L-glutamine, heparin sulfate, hydrocortisone, fetal bovine serum, and ascorbic acid. To prepare the RFP-GMEC and GMEC media, the EGM-2 SingleQuots pack was added to 500 mL of Lonza EBM-2. The SingleQuotes pack contained: human epidermal growth factor, hydrocortisone, gentamicin/amphotericin-B, fetal bovine serum, vascular endothelial growth factor, human fibroblast growth factor beta, R^3 insulin growth factor-1, and ascorbic acid.

Conditioned medium was culture medium collected from a culture of PTEC-Terts after it had been in the culture flask for two days. The conditioned medium contained all exogenous factors secreted by the PTEC-Terts. When collected from a 3D-perfused PTEC-Tert culture, the conditioned medium was referred to as being "from chip." When collected from a static 2D culture of PTEC-Terts in a T225 Corning flask, it was referenced with the phrase "from flask."

Biomaterials

Extracellular Matrix

The extracellular matrix (ECM) material consisted of a cross-linked hydrogel, colloquially termed "gelbrin" by the Lewis Laboratory. This biomaterial was prepared as previously described [8]. In short, the constituents of the extracellular matrix included: gelatin, fibrin, PBS without Ca^{2+} or Mg^{2+}, $CaCl_2$, transglutaminase (TG), and thrombin. The components were combined at different volumetric amounts to form ECM with varied swelling behaviors, and these specific formulations have been reported for each experiment. The first step in creating the hydrogel involved mixing the gelatin, fibrin, PBS, and $CaCl_2$ together at 37°C. TG was then added to the homogeneous mixture and permitted to slowly crosslink the gelatin and fibrin during a 15-minute incubation period at 37°C. After the 15 minutes passed, the entire solution was mixed with thrombin to initiate a rapid cross-linking step. The twice cross-linked hydrogel was then incorporated into the tissue construct as the ECM material.

Biocompatible Ink

The biocompatible, fugitive ink used to 3D print the channel geometries consisted of Pluronic F127 and 1X PBS without Ca^{2+} or Mg^{2+}. The inks were prepared by adding the powdered Pluronic to the PBS to form solutions that were 35 or 38 percent Pluronic by weight. The solutions

were mixed for five minutes at 2000 rpm using a planetary centrifugal mixer manufactured by Thinky. They were then cooled to 4°C for approximately 10 minutes prior to additional mixing. The mixing and cooling process was repeated until the mixture appeared to be homogeneous. The solutions were refrigerated at 4°C overnight prior to insertion into syringes for printing. Before they were deployed for printing, the filled ink dispensers were centrifuged a final time to eliminate remaining air bubbles.

Chip Materials

Perfusion System

The system for perfusing tubule structures with media involved rubber tubing, a peristaltic pump, and encasing for the tissue culture environment (figure 2). The peristaltic tubing was 2-Stop PharMed BPT Tubing produced by Cole-Parmer Instrument Company. The silicone tubing was Versilon SPX-50 silicone tubing. The chips themselves were contained within metal and acrylic plates adhered to the PDMS gasket using metal screws.

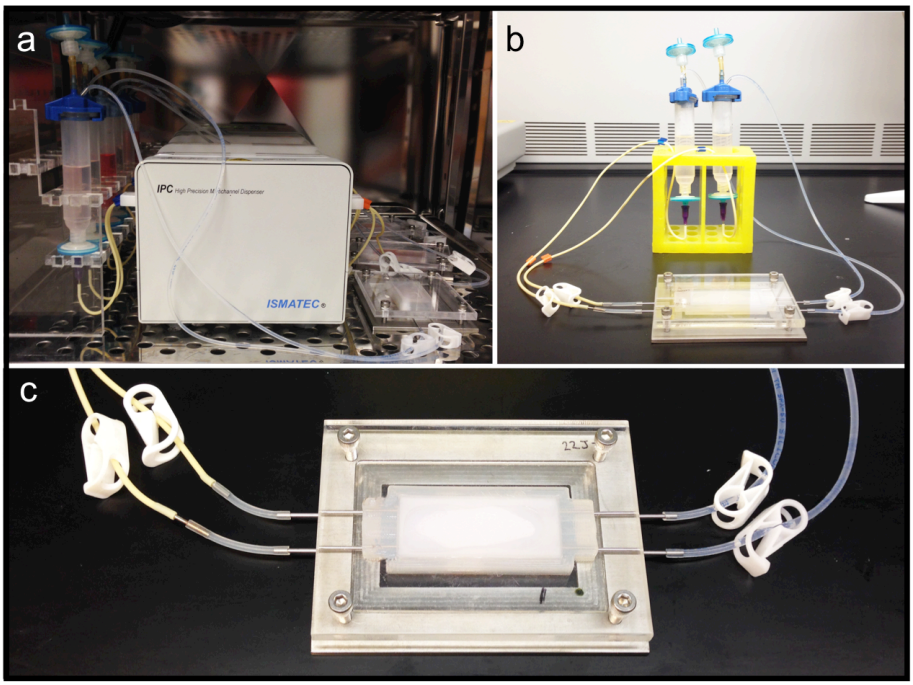

Figure 2: Perfusion system for culturing 3D-bioprinted tissue constructs. Figure (a) indicates setup of the chip on the peristaltic pump. Figure (b) illustrates the closed-loop system for media flow. Figure (c) shows an aerial view of a 3D-printed construct contained within a PDMS perimeter and encased within acrylic and metal plates (here, the tubules are not macroscopically visible through the opaque extracellular matrix). Media enters the channels through the yellow peristaltic and metal perfusion tubes visible on the left-hand side of the photograph, flows through the bioprinted tubules, and exits through the metal and silicone tubes on the right-hand side.

Flow was controlled through the tubing using plastic clips. Metal tubes purchased from Microgroup at varying inner and outer diameters were used to interface with the bioprinted tubules to create channel inlets and outlets. Culture media was contained within syringes purchased from Nordson and dispensed through nozzles also produced by Nordson. Filters were used to improve sterility of the culture environment. The entire system was contained within a VWR incubator at 37°C and 5% CO_2.

Polydimethylsiloxane (PDMS) Ink

The PDMS ink used to 3D print the PDMS container for the tissue construct was formed by combining Dow Corning SE 1700 base and catalyst in a 10:1 base-to-catalyst ratio. The mixture was then centrifuged in a planetary centrifugal mixer for three minutes at 2000 rpm prior to loading in a syringe. The filled syringe was then centrifuged for five minutes at 5000 rpm to remove remaining air bubbles.

III. Methods

Chip Construction and Maintenance

The 3D tissue construct containing epithelialized or endothelialized channels consisted of four principal components: the polydimethylsiloxane (PDMS) gasket, the extracellular matrix, the cellularized tube, and the outer containment system that permitted incubation and perfusion (figure 2). Both the PDMS container and the tubular geometries were created by directly depositing layers of material through 3D printing, while the ECM and chip encasement were manually assembled. Preparation and assembly of these components are described below.

Cellular Culture

Cells were cultured according to the respective manufacturers' protocols, excluding custom protocols developed for PTEC-Terts, and cell culture media were changed every two to three days. Cells were visually monitored every two days for morphological changes.

Generation of G-Code for the 3D Printers

All automatic functional capabilities of the 3D printers were controlled using custom G-code. G-code is a numerical control programming language that determines the print paths, speeds, and extrusion pressures employed by 3D printers to deposit filaments in a tightly controlled manner. The G-codes used to 3D print the PDMS container and tubular architectures were developed using MATLAB. Dr. Mark Skylar-Scott kindly provided the modular code for designing the PDMS containers.

Chip Construction and Assembly

The first step to create the perfusion chip involved 3D printing the PDMS border using G-code and materials as described above. The PDMS was printed onto a 2"x3" glass slide using a nozzle whose inner diameter (ID) measured 410 μm. The printed gasket was then cured for at least one hour at 70°C. The PDMS gasket, clear tubing, media reservoirs, plastic clips, and metal components were autoclaved prior to assembly into the tissue construct. Since the other chip materials were not autoclavable, they were cleansed thoroughly by washing with 70% ethanol and deionized water.

After the materials were sterilized, a thin layer of gelbrin was used to coat the glass slide that formed the bottom of the PDMS gasket. The hydrogel was permitted to dry slightly, producing a level, semi-rigid surface on which to print the tubules. Prior to printing, four metal tubes with outer diameters (OD) of 800 μm were inserted into the gasket and four smaller metal tubes with ODs of 300 μm were nested inside of the outer tubes. The tubes protruded a few millimeters into the gasket

but permitted printing on the exposed ECM substrate. Two lines representing the proximal tubule and the vasculature were then printed onto the dried ECM using the Pluronic F127 ink extruded through a 200 μm-diameter nozzle (figures 3ai, 3bi). The architecture of the printed lines was such that the metal tubes could be physically connected to the beginnings and ends of the pathways to allow later integration into the perfusion system. The printed structures were then quickly encapsulated within the ECM hydrogel to prevent drying of the Pluronic and to form the extracellular matrix of the tissue construct (figures 3aii, 3bii). The construct was then incubated at 37°C for at least one hour to permit full crosslinking of the ECM. The added ECM material rehydrated the base layer, and the slow nature of the TG crosslinking permitted lamination of the two layers.

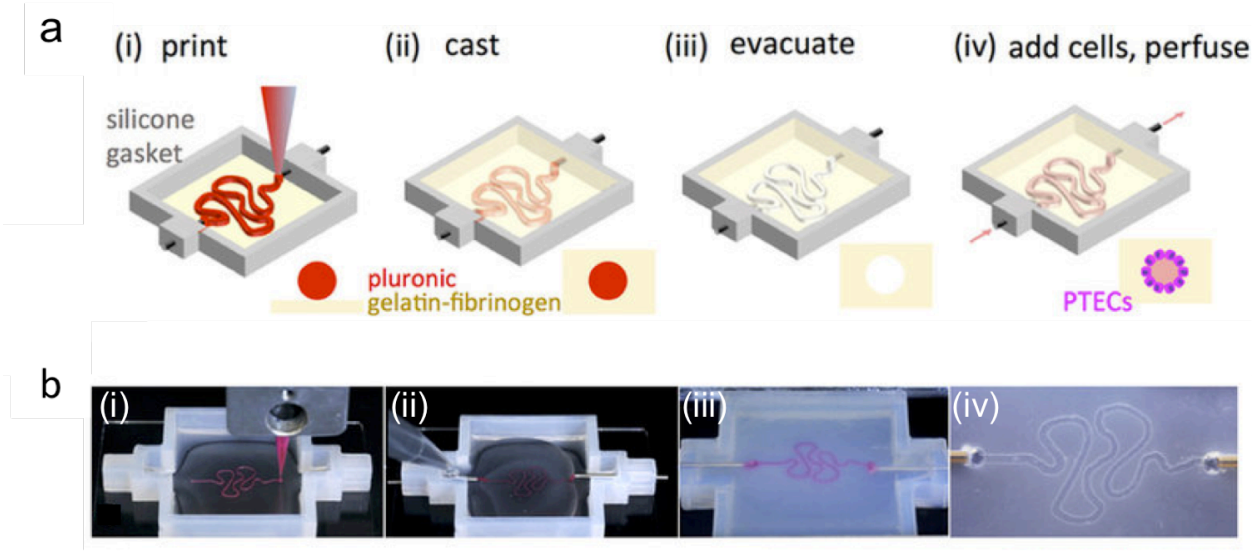

Figure 3: Printing a tubule embedded within an extracellular matrix. Figure (a) illustrates the process of printing Pluronic F127 fugitive ink onto an ECM substrate (i), casting ECM on top of the printed geometry (ii), evacuating the fugitive ink (iii), and ultimately seeding the tubule with cells for culture under perfusion (iv). Figure (b) provides images of the same process, in which (i) demonstrates printing with Pluronic F127 fluorescently labeled for visualization, (ii) shows casting of the ECM, (iii) depicts the construct prior to evacuation, and (iv) reveals the construct post-evacuation.

Following incubation, the construct was cooled at 4°C for 20 minutes to liquefy the Pluronic F127 ink. The liquefied ink was evacuated from the construct through removal of the inner metal tubes (figures 3aiii, 3biii-iv), yielding two tubular channels embedded within the ECM. Peristaltic tubing was connected to each of the four remaining metal outer tubes to form two sets of independently addressable inlets and outlets for the channels. Prior to attachment to the tissue construct, the tubing was pre-filled with culture medium to prevent the admission of air bubbles into the channels. Any remaining air and Pluronic ink were flushed out of the channels prior to closing the perfusion system. Each set of tubing was connected to a single reservoir containing culture

medium such that two closed-loop circuits were formed; each circuit consisted of a culture medium reservoir, peristaltic tubing that led to the channel inlet, the embedded channel itself, and clear tubing that connected the channel outlet back to the medium reservoir. Filters were attached to the media reservoirs to promote sterility and plastic clips were attached to the tubes to enable a method of obstructing flow (i.e., during media changes). The entire construct was encased within a metal plate and an acrylic plate that were sealed against the PDMS gasket using metal screws (figure 2). This fabrication process was performed for tubules of varying geometries (figure 4).

After construction, the chips were connected to a peristaltic pump such that the pump forced media to flow from the reservoirs, through the inlet tubing, and into the channels. The displacement of fluid through the channels forced the fluid to move through the outlet tubing and back into the media reservoirs for recycling through the circuit (figure 2). The speed of the pump was altered to produce different shear stresses through the channels.

Cell Seeding of the Bioprinted Channels

The embedded channels were populated with epithelial or endothelial cells. PTEC-Terts were seeded into the channels at a cell density of 35 million cells/mL, while RFP-GMECs and GMECs were seeded into the channels at densities of 10 or 15 million cells/mL. Following seeding, the cells were incubated overnight in the channels at 37°C without flow to permit adhesion to the extracellular matrix. Un-adhered cells were then lightly flushed from the channel and perfusion was initiated.

Pin Pullout Technique to Generate Channels

In the pin pullout technique, used to produce embedded channels within the ECM, four metal tubes were initially inserted into the gasket to form the inlets and outlets for two parallel lines. Two longer and thinner metal tubes were then inserted into these four outer tubes to span the length of the gasket. The outer diameter of the inner tubes became the outer diameter of each evacuated channel. The gelbrin was directly cast around the pins and processed according to the same protocols reported for bioprinting. After the ECM was fully cross-linked, the inner tubes were carefully removed to form the perfusable channels.

MTS Assay

The MTS Cell Proliferation assay is a tetrazolium reduction assay that measures cell viability through determination of cellular metabolic activity. The colorimetric assay depends on the use of MTS tetrazolium, a tetrazolium compound that dissolves in culture medium. Metabolically active cells reduce MTS tetrazolium into a formazan dye that absorbs wavelengths of light between 490 and 500 nm. Samples that demonstrated significant amounts of light absorption in the culture medium above the cells therefore produced high quantities of formazan, indicating healthy cellular metabolic functioning, while samples that resulted in poor light absorption demonstrated low cellular metabolic and proliferative activity.

The MTS Assays were performed using the CellTiter 96® AQueous Non-Radioactive Cell Proliferation Assay (ref. #G5421) produced by Promega. The kit contained MTS solution at 2.0 mg/mL in Dulbecco's phosphate buffered saline, pH 6.0. Prior to performing the assay, all media was removed from each culturing well. Fresh media was added to each well at 500 μL in the 24-well culturing plates and 200 μL in the Transwell inserts. MTS solution was added at a 100 μL in the lower wells and 70 μL in the insert wells. After a 1-hour incubation with the MTS solution at 37°C, the first MTS assay of a given session was performed using a BioTek Synergy HT plate reader. Successive assays were performed after subsequent incubation intervals. All data was exported from the software to Microsoft Excel.

Graphical and Statistical Analysis of the MTS Assays

All MTS Assay data were exported from Excel and graphed using MATLAB R2014b or Mathematica. In most cases each data set provided the mean and standard deviation of nine recorded optical densities at 490 nm per well. If the mean and standard deviation had not been provided, they were calculated from the three repeated optical density measurements recorded per well using built-in functions in MATLAB R2014b. Repeated measurements within an individual well represented technical replicates while multiple wells cultured using the same media conditions represented biological replicates. The sample mean and sample standard deviation were computed for the technical replicates before using these values to compute the sample mean and sample standard deviation for the biological replicates. The sample means and sample standard deviations were normalized to the positive control prior to graphing. Reported error bars represent the standard deviations of the biological replicates, since the technical replicates' standard deviations were negligible.

Setup and Culturing Conditions

MTS assays were conducted in standard 24-well culturing plates and in Transwell 24-well culturing plates. In all experiments, each plate was seeded entirely with a single cell type and referred to by its cellular name (i.e. a "HUVEC-Tert plate" indicates a plate seeded entirely with HUVEC-Terts). For the non-Transwell experiments, the plates were seeded with HUVEC-Terts, PTEC-Terts, or RFP-GMECs directly onto the tissue culture plastic. The 24-well Transwell culture plates consisted of a bottom layer of culturing wells that resembled a standard 24-well plate and an insert layer that consisted of 24 smaller wells with permeable membranes. Each of the membranes rested above the bottom layer to enable culture of one cell type with one medium in the bottom layer and culture of another cell line with a second medium in the top layer. The permeability enabled bidirectional fluid movement between the two layers, potentially transporting secreted factors from one culture to the other. For the Transwell experiments, the base wells were seeded with either PTEC-Terts or primary PTECs while the insert wells were seeded with RFP-GMECs.

Positive and negative controls were incorporated into each of the MTS assays. The positive control took the form of the culture medium corresponding to the plate's seeded cell type while the negative control took the form of the culture medium corresponding to the second cell type probed for co-culturing compatibility with the seeded type. In some experiments, a mixture of the media formulations was prepared by combining the two media in a 1:1 volumetric ratio. Media formulations were also prepared by adding the specific supplemental media components from the seeded cell type to the opposing culture medium at the same concentration it constitutes in its native medium. In the Transwell plates, the bottom layer could be cultured in different medium than the insert wells. Six or eight media conditions were tested in each experiment with four or three biological replicates, respectively.

MTS Assays for HUVEC-Tert and PTEC-Tert Compatibility

In the first series of MTS assays (figure 5), HUVEC-Terts were cultured in PTEC-Tert media conditions while PTEC-Terts were cultured in HUVEC-Tert media conditions. Two plates were included in the first set of assays (figures 5a-b), which assessed the individual effects of discrete supplemental media components on the opposing cell line. The following PTEC-Tert media components were tested in isolation: insulin-transferrin-selenium (ITS, Sigma ref. #13146-5ML), prostaglandin E_1 (PE1, Sigma ref. #P5515), triiodothyronine (T3, Sigma ref. #T-5516), and sodium selenite (SS, Sigma ref. #S-9133). The following HUVEC-Tert media components were tested in isolation in their respective dilution as recommended by the manufacturer: recombinant human

vascular endothelial growth factor (rhVEGF), recombinant human epidermal growth factor (rhEGF), recombinant human insulin-like growth factor (rhIGF-1), hydrocortisone (HC), and heparin sulfate (HS), all selected from the EGM-2 SingleQuots pack produced by Lonza (catalogue #CC-4176). In both plates, aprotonin (Apo, EMD-Millipore, VWR ref. #80603-220) was tested at a 1% volumetric concentration in base medium because the Lewis Laboratory's culturing protocol for 3D-perfused chips includes adding 1% aprotonin to the culture medium. These assays were performed on day seven of culture.

Rather than testing the components individually, the second set of MTS assays (figure 5c-d) examined the synergistic effects of combining the media supplements into single formulations. In these assays, the components were collectively added to base media. The HUVEC-Tert components that were combined with PTEC-Tert base medium included: rhVEGF, rhEGF, rhIGF-1, HS, HC, human recombinant fibroblast growth factor (rhFGF), ascorbic acid (AA), and L-glutamine. The PTEC-Tert components that were added to HUVEC-Tert base medium included: ITS, T3, SS, PE_1, HC, AA, and Geneticin® (G418). All components were added at the concentrations at which they occur in their respective culture media. These assays were performed on day seven of culture.

MTS Assays for RFP-GMEC and PTEC-Tert Compatibility

In this set of MTS assays (figure 6), RFP-GMECs were analyzed for their viability relative to HUVEC-Terts when exposed to components of PTEC-Tert medium. Unlike the media used in the HUVEC-Tert and PTEC-Tert MTS assays, the PTEC-Tert culture medium used in these assays excluded G418 because G418 produces known cytotoxic effects. The first of the two MTS assays (figure 6a) primarily utilized chip-conditioned PTEC-Tert culture medium, while the second MTS assay (figure 6b) utilized flask-conditioned PTEC-Tert culture medium. The other media formulations remained identical between the two assays. These assays were performed on days seven (figure 6a) and six (figure 6b) of culture.

MTS Assays for PTEC-Tert, Primary PTEC, and RFP-GMEC Compatibility

MTS assays were performed using Corning Transwell permeable culture plate inserts to assess cellular viability during co-culture of PTEC-Terts and RFP-GMECs. Primary PTECs were also examined in co-culture with RFP-GMECs to determine whether the primary cells improved RFP-GMEC viability relative to PTEC-Terts. The Transwell assays were performed with and without extracellular matrix coatings to determine whether the gelbrin differentially affected cellular viability. In all of the Transwell plates, positive controls were constructed for both cell types by

seeding either the plate or insert well with its respective cell type and leaving the other well unseeded. The RFP-GMECs were consistently seeded at a density of 16,000 cells/cm^2 and the PTECs (both the primary and immortalized lines) were seeded at a density of 80,000 cells/cm^2. Both cell types were seeded concurrently. In all cases, 500 μL of media were used in the bottom well and 150 μL of media were used in the insert. The MTS assays were performed on day seven of co-culture.

The first set of Transwell MTS assays (figure 7a) consisted of two Transwell plates. In the first column, representing the positive control for PTECs, both the base and insert wells were cultured in PTEC culture medium. In the second column, which provided the positive control for RFP-GMECs, both wells were cultured in RFP-GMEC culture medium. Each cell type was cultured independently with its native culture medium in the third condition. In the fourth condition, both cell types were cultured with 1:1 volumetric primary PTEC culture medium to GMEC culture medium. In the fifth condition, both cell types were cultured in primary PTEC culture medium. In the sixth condition, both cell types were cultured in GMEC culture medium.

Immunostaining and Imaging

Immunostaining Static 2D Samples

First, 2D static samples were washed twice with PBS containing Ca^{2+} and Mg^{2+}. Next, the cells were fixed in formalin for approximately 30 minutes. The formalin was then removed and the cells were washed three times with PBS containing Ca^{2+} and Mg^{2+}. After the last wash was removed, the samples were blocked overnight at 4°C in a PBS solution consisting of 1% donkey serum and 0.25% Triton-X. Samples were then washed once with PBS containing Ca^{2+} and Mg^{2+}. Primary antibodies were diluted 1:250 in staining solution containing 0.5% bovine serum albumin (BSA) and 0.125% TritonX in PBS containing Ca^{2+} and Mg^{2+}, and staining occurred overnight at 4°C. Prior to staining with secondary antibodies, the samples were washed three times for five minutes each with PBS containing Ca^{2+} and Mg^{2+} and placed at 4°C overnight. Secondary antibodies were diluted 1:500 in staining solution and stained for 2-5 hours before staining for 4',6-diamidino-2-phenylindole (DAPI) at a dilution of 1:1500 from an original concentration of 1 mg/mL and actin at a dilution of 1:500 from the stock solution (see table 1). After 30 minutes, the samples were washed three times with PBS containing Ca^{2+} and Mg^{2+} and stored at 4°C in tween prior to confocal imaging.

Immunostaining 3D-Perfused Chips

Chips were initially perfused with PBS containing Ca^{2+} and Mg^{2+} for a maximum of 15 minutes to displace remnant media from the chips. Next, the chips were perfused with approximately 6 mL of formalin to fix the cells inside of the channels and the entire chip was excised from its housing and bathed in formalin for 20 – 30 minutes. Afterwards, the samples were washed three times in PBS containing Ca^{2+} and Mg^{2+} before blocking overnight at 4°C in solution containing 1% donkey serum and 0.25% Triton-X in PBS containing Ca^{2+} and Mg^{2+}. The samples were then washed one more time with PBS containing Ca^{2+} and Mg^{2+}. Primary antibodies were diluted 1:250 in staining solution containing 0.5% bovine serum albumin (BSA) and 0.125% TritonX in PBS containing Ca^{2+} and Mg^{2+}, and staining occurred overnight at 4°C.

Antibody or Stain	Source	Catalogue Number	Concentration
Na^+/K^+ ATPase	abcam	ab76020	1:250
K Cadherin	abcam	ab68342	1:250
Von Willebrand Factor	abcam	ab68545	1:250
VE Cadherin	abcam	ab7047	1:250
Acetylated Alpha Tubulin	abcam	ab9498	1:250
CD31	abcam	ab28364	1:250
Megalin	abcam	ab76969	1:250
LTL	Vector Lab	SP-2002	4 drops per mL
NucBlue	Life Technologies	R37605	1:500
Streptavidin, Alexa fluor 514 conjugate	Life Technologies	S32353	1:500
Alexa fluor 555	Thermo Fisher Scientific	A31572	1:500
Alexa fluor 488	Thermo Fisher Scientific	A21202	1:500
Alexa fluor 647 phalloidin	Thermo Fisher Scientific	A22287	1:500

Table 1: Immunostaining reagents. This table delineates all antibodies and stains used in immunostaining.

Prior to staining with secondary antibodies, the samples were washed three times for 15 – 30 minutes each with PBS containing Ca^{2+} and Mg^{2+} and placed at 4°C overnight. Secondary antibodies were diluted 1:500 in staining solution and stained for multiple hours before staining with DAPI at a dilution of 1:1500 from a stock solution of 1 mg/mL. After 30 minutes, the samples were washed three times for 15 – 30 minutes each with PBS containing Ca^{2+} and Mg^{2+} and stored at 4°C in tween prior to confocal imaging.

Confocal Imaging and Imaging Analysis

Confocal imaging was performed using Zen 2011 software and a Zeiss laser scanning confocal microscope. Images were post-processed using Imaris software and ImageJ.

PTEC-Tert and RFP-GMEC Morphology and Expression in 2D Static Culture

Static controls (figures 8-10) were prepared to evaluate cellular expression in response to three different gelbrin formulations, representing the extracellular matrix, and relative to 3D-perfused environments. PTEC-Terts and RFP-GMECs were individually cultured in a distinct set of 6-well plates, creating six conditions for each cell type with two biological replicates each. Three distinct gelbrin formations were included to enable comparison of the three differential ECM compositions used throughout this thesis. These conditions are summarized below:

Condition	Formulation
Tissue culture plastic	Cells cultured directly in wells, without gelbrin.
Gelatin and transglutaminase	Cells cultured on 4.5 wt% gelatin prepared in PBS, combined with 0.2 wt% transglutaminase. Thrombin and fibrin were excluded from the formulation.
Fibrin	Cells were cultured on 40 mg/mL fibrin solution prepared in PBS.
Gelbrin 1	Gelbrin containing 1 wt% gelatin, 25 mg/mL fibrin, and 2 units/mL thrombin.
Gelbrin 2	Gelbrin containing 4.5 wt% gelatin, 40 mg/mL fibrin, and 2 units/mL thrombin.
Gelbrin 3	Gelbrin containing 7.5 wt% gelatin, 40 mg/mL fibrin, and 1 unit/mL thrombin.

Table 2: Extracellular matrix and substrate formulations for examining cellular morphology in 2D static culture.

PTEC-Tert and RFP-GMEC Morphology and Expression in 3D-Perfused Culture

Two chips (figures 10-13) were created containing two perfusable lines each. Gelbrin was used as the extracellular matrix material and was prepared according to protocols described previously. The gelbrin formulation in these particular chips consisted of 1 wt% gelatin, 25 mg/mL fibrin, and 0.2 wt% transglutaminase (Gelbrin 1). The inner metal perfusion pins used in these chips had an outer diameter of 300 μm and were perfused under a flow rate of 2 μL/min, exposing the cells to a shear stress of 2.5509 dynes/cm^2. The PTEC-Terts were seeded after 2 days of media perfusion as described above. The PTEC-Terts were cultured using PTEC-Tert culture medium with 1% aprotonin and 1% antibiotic-antimycotic solution. The RFP-GMECs were seeded 5 days

after PTEC seeding and cultured using GMEC culture medium with 1% aprotonin and 1% antibiotic-antimycotic solution. G418 was excluded from both culture media. The chips were fixed in formalin after the PTECs had been in culture for a total of 10 days and the GMECs had been in culture for 5 days. Morphological features from Homan *et al.* [9] on Gelbrin 3 were also studied (figure 14).

In the chips produced via the glass pin-pullout method, the chips were seeded with PTEC-Terts and perfused in the incubator for one month prior to fixing in formalin and staining for TEM imaging. The TEM imaging was kindly performed by Dr. Kimberly Homan.

Locked-Nucleic Acid (LNA) Transport Assay

Three chips were 3D printed using the design depicted in figure 4a with an extracellular matrix formulation containing 4.5 wt% gelatin, 40 mg/mL fibrin, and 2 units/mL thrombin (Gelbrin 2). The tubule diameters measured 350 μm. One tubule of each chip was seeded with PTEC-Terts while the other channels were left unseeded. Both chips were perfused using PTEC-Tert culture medium for four weeks in the incubator prior to performance of the LNA test. Nine days prior to conducting the assay, fetal bovine serum (FBS) was added to the medium at a volumetric concentration of 3%. To perform the assay, tool LNA-Alexa647 at 500 nM was perfused into either the proximal tubule line, for apical access, or the empty secondary line, for basal access. The tubules were then flushed with 3 mL of LNA-free media for approximately 30 minutes prior to fixing in formalin. Chips were counterstained with a Na^+/K^+ ATPase antibody and DAPI. Two of the tubules were perfused either basally or apically with LNA for 24 hours (figures 15a, 15f-m) and imaged following perfusion. The other chip was perfused basally for six hours and imaged every two hours during this time (figures 15b-e).

IV. Results

Design of the Vascularized Model of the Convoluted Proximal Tubule

Developing the Model

The first iteration of the vascularized proximal tubule model appears in figure 4a. This design permitted proximity of the two independently addressable channels without introducing external variables, such as curvature of the proximal tubule line, into the system. Vascular cells were cultured in one line while proximal tubule epithelial cells were cultured separately in the other. The design further enabled the study of endothelial and epithelial cell functionality in 3D perfused culture, including differential behavior of the cells in 2D versus 3D culture, in static versus flowing media, and molecular transport capabilities. The associated MATLAB script used to generate G-Code for the printed geometry possessed capabilities for dynamically customizing the tubular channel lengths and inter-channel distance. A secondary advantage of the design depicted in figure 4a relative to the designs depicted in figures 4b and 4c was that it could be rapidly reproduced using the pin pullout method.

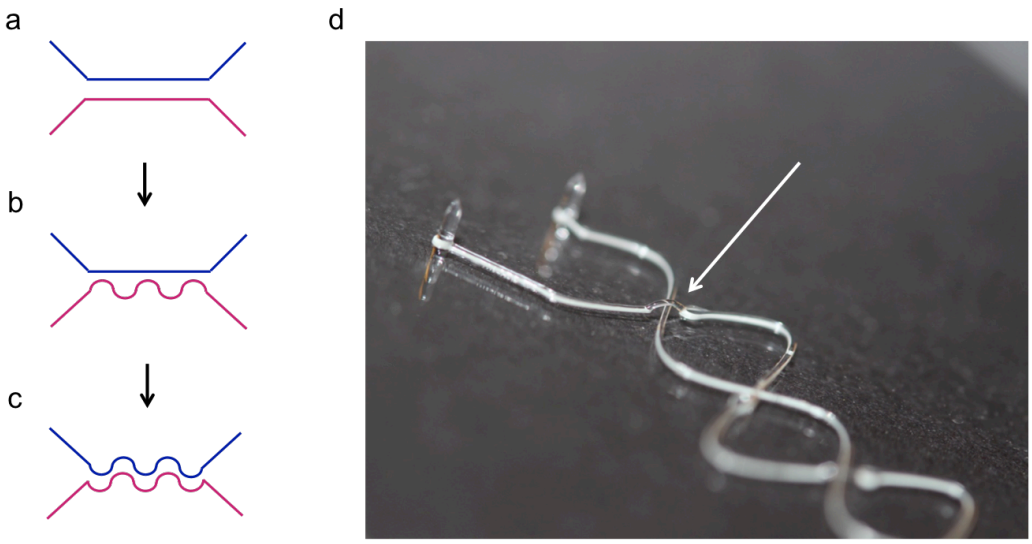

Figure 4: Evolution of the vascularized proximal tubule model. This figure demonstrates the progression of past, current, and future vascularized proximal tubule designs. Figure (a) demonstrates the initial vascularized model, incorporating two adjacent channels, which was used to conduct the locked-nucleic acid uptake assay. Figure (b) demonstrates the introduction of curvature into the model to produce the vascularized PT explored throughout this thesis. Future directions for the vascularized model are depicted in (c) and (d). The arrow in (d) indicates spatial elevation to print a vascular line above the proximal tubule line. Figure (d) was created by Dr. Homan.

The second design, illustrated in figure 4b, simulated the convoluted nature of the proximal tubule by introducing curvature into the proximal tubule channel. Like the design depicted in figure 4a, the G-code for this design could be readily modified to accommodate different channel

lengths and interstitial distances. The sinusoidal nature of the proximal tubule line created regions of enhanced and diminished proximity to the vascular line, allowing comparative analysis of proximity within a single chip sample. The symmetry of the sinusoid itself introduced technical replicates within each chip. These took the form of three replicates for studying proximity to the vascular line, represented by the peak of each sinusoidal period, and two replicates for analyzing decreased proximity.

Selection of the Renal and Vascular Cell Lines

After initial cellular death was observed in 3D-perfused co-culture of HUVEC-Terts and PTEC-Terts (described below), it was necessary to identify an alternative vascular cell line that would be compatible with PTEC-Terts in the vascularized PT system. 2D cultures offered surrogate environments for robustly screening cellular viability, expression, and morphological appearances prior to translation into 3D chip constructs.

HUVEC-Terts in 3D-Perfused Co-Culture with PTEC-Terts

Initially, two vascularized models of the proximal tubule were printed and seeded with PTEC-Terts in the proximal tubule line and HUVEC-Terts in the vascular line. The HUVEC-Terts were seeded on the sixteenth day following initial seeding of the PTECs. In one of these chips, the HUVEC-Terts died by the sixth day in co-culture with the PTEC-Terts while the PTEC-Terts remained viable. In the other chip, the PTEC-Terts died by the fourth day in co-culture while the HUVEC-Terts appeared healthy. In the latter case, the extracellular matrix and proximal tubule channel appeared to show evidence of contamination. Evidence of contamination was not observed in the first chip, suggesting that internal factors such as media incompatibilities may have contributed to cellular death of the vascular cell line.

MTS assays were next performed to determine whether individual components of the media, synergistic effects of the components within the media, or secretions by one cell line into the media produced cytotoxic effects on the opposing cell line. The assays sought to examine the effects of culturing a vascular cell line with the media corresponding to a renal cell line, as well as the converse culturing relationship. The purpose of these experiments was to assess the potential for compatibly co-culturing the two cell types together in the 3D-perfused vascularized renal proximal tubule model, where both cell types would be exposed to the other cell line's culture medium, respectively.

PTEC-Tert Media Lowers Viability of HUVEC-Terts

The first set of MTS assays (figures 5a-b) assessed whether individual components of the PTEC-Tert media produced specific cytotoxic effects on the HUVEC-Tert cell line and vice versa. It was found that individual components did not yield a significant reduction in cell viability relative to the positive control, preventing the conclusion that an individual PTEC-Tert medium component was primarily responsible for the HUVEC-Tert death observed in 3D-perfused culture. However, the 1:1 combined PTEC-Tert and HUVEC-Tert culture medium elevated the cellular metabolic activity of the HUVEC-Tert cells (figure 5a), suggesting that the cells may have demonstrated signs of metabolic stress when exposed to a combination of the two media, although these results were non-signficant. Similarly, individual PTEC-Tert medium components appeared to metabolically and morphologically enhance HUVEC-Tert metabolic stress. It was further observed that the HUVEC-Tert media negligibly impacted the PTEC-Tert viability (figure 5b). Although HUVEC-Tert media non-significantly diminished the PTEC-Tert metabolic activity relative to the positive control, a 1:1 mixture of the two culture media slightly elevated the metabolic activity, suggesting induced stress similar to that observed in the HUVEC-Tert plate (figure 5a). Individual components of the HUVEC-Tert culture media did not appear to significantly decrease cellular viability or proliferative behavior of the PTEC-Terts.

Since individual components did not appear to invoke cellular death, the next set of MTS assays (figures 5c-d) investigated whether the base media produced cytotoxic effects. When used as the only culturing agent, PTEC-Tert base medium resulted in nearly complete HUVEC-Tert cellular death. Since cellular death was also observed when HUVEC-Terts were cultured in HUVEC-Tert base medium, it was concluded that HUVEC-Tert medium components were necessary for cellular viability. When HUVEC-Tert medium components were added to the PTEC-Tert base medium to replicate conditions found in the 3D perfused vascular line of preexisting chips, the cellular metabolic activity was elevated to levels approximately 20% greater than the control. This result, in conjunction with the elevated metabolic stress observed in mixed culture media (figure 5a), suggested that the PTEC-Tert base medium itself contained components that adversely affected normal HUVEC-Tert functionality but did not lead to death in the presence of HUVEC-Tert culture medium components. Conversely, adding PTEC-Tert culture medium components to HUVEC-Tert culture medium resulted in significant cellular death. Taken together, these results suggest that synergistic effects of the PTEC-Tert culture medium components (in absence of their own HUVEC medium components) produced the cellular death observed in the 3D-perfused

vascular line.

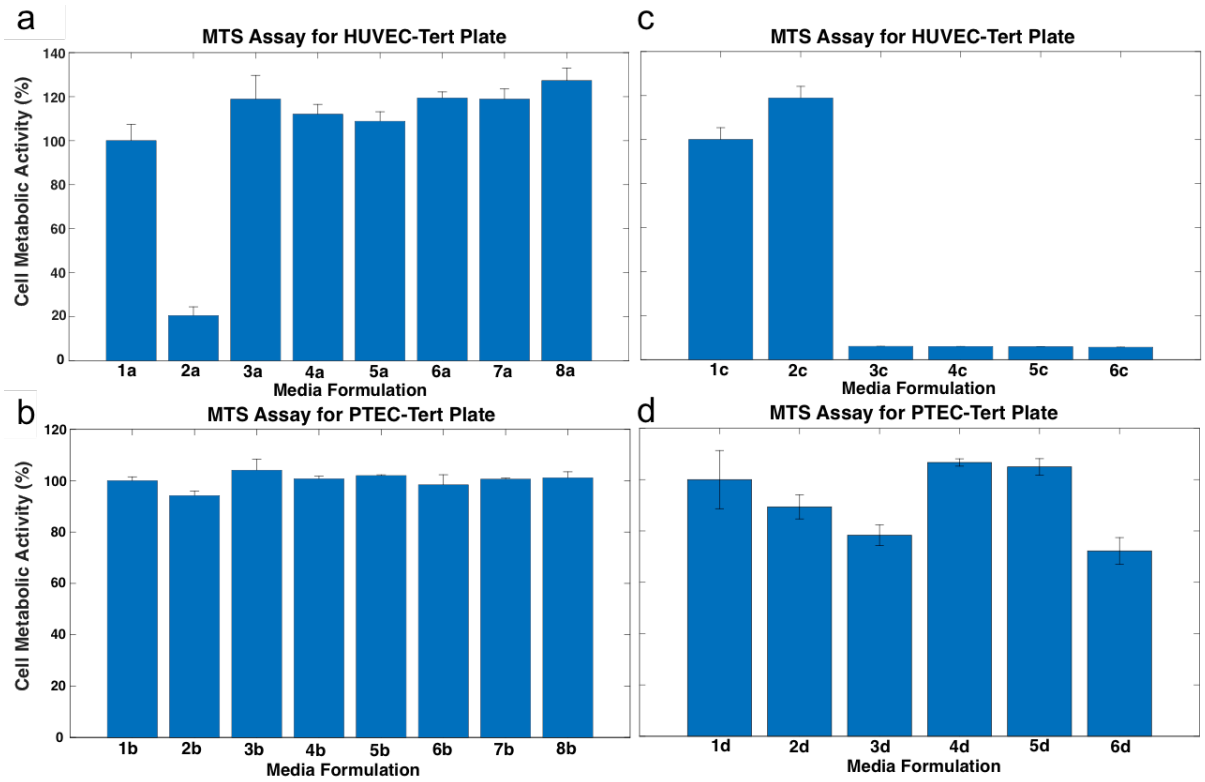

Medium Condition	Formulation	Medium Condition	Formulation
1a	HUVEC-Tert culture medium	**7b**	Hydrocortisone
2a	PTEC-Tert culture medium	**8b**	Heparin sulfate
3a	1:1 HUVEC-Tert:PTEC-Tert culture medium	**1c**	HUVEC-Tert culture medium
4a	Insulin-transferrin-selenium	**2c**	PTEC-Tert base medium with HUVEC-Tert components
5a	Prostaglandin E_1	**3c**	PTEC-Tert base medium
6a	Sodium selenite	**4c**	PTEC-Tert culture medium
7a	Aprotonin	**5c**	HUVEC-Tert base medium with PTEC-Tert components
8a	Triiodothyronine	**6c**	HUVEC-Tert base medium
1b	PTEC-Tert culture medium	**1d**	PTEC-Tert culture medium
2b	HUVEC-Tert culture medium	**2d**	HUVEC-Tert base medium with PTEC-Tert components
3b	1:1 HUVEC-Tert:PTEC-Tert culture medium	**3d**	HUVEC-Tert base medium
4b	Recombinant human vascular endothelial growth factor	**4d**	HUVEC-Tert culture medium
5b	Recombinant human insulin-like growth factor	**5d**	PTEC-Tert base medium with HUVEC-Tert components
6b	Recombinant human epidermal growth factor	**6d**	PTEC-Tert base medium

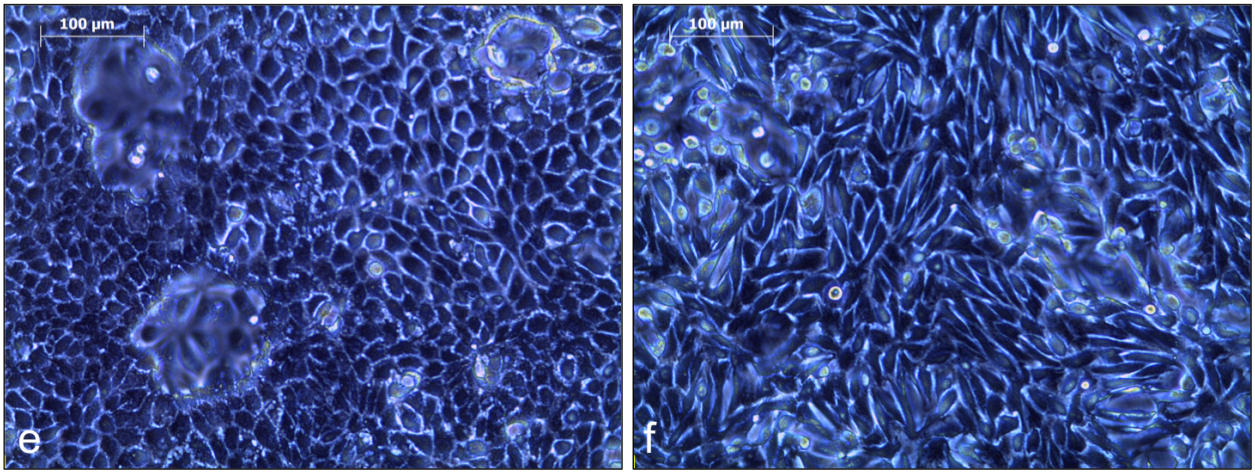

Figure 5: Synergistic PTEC-Tert culture medium effects result in HUVEC-Tert death.

Graphical representation of the MTS assays conducted for HUVEC-Terts cultured in PTEC-Tert media formulations (a, c) and for PTEC-Terts cultured in HUVEC-Tert media formulations (b, d). "CM" refers to "culture medium," "BM" refers to "base medium," and "com." refers to "components. All assays were conducted after the cells had been in culture for seven days. Figure (e) shows PTEC-Terts cultured in PTEC-Tert culture medium and figure (f) shows PTEC-Terts cultured in HUVEC-Tert culture medium, with scale bars of 100 µm.

Antagonism of HUVEC-Terts by PTEC-Tert Media is Unidirectional

The second set of MTS assays demonstrated that HUVEC-Tert medium did not substantially affect PTEC-Tert cellular metabolic activity (figure 5d). Notably, little difference in viability occurred between PTEC-Terts cultured in PTEC-Tert base medium with added HUVEC-Tert components and PTEC-Terts cultured entirely in HUVEC-Tert culture medium. The comparable cellular metabolic activity levels between PTEC-Terts cultured in PTEC-Tert culture medium and PTEC-Terts cultured in PTEC-Tert culture medium with added HUVEC-Tert components suggested that PTEC-Tert components could be replaced by HUVEC-Tert components in a PTEC-Tert culture with minimal differences in viability. However, the PTEC-Tert morphology became irregularly elongated from its confluent cuboidal form (figure 5e) when exposed to the HUVEC-Tert medium (figure 5f).

In both cases, the cellular metabolic activity was elevated only slightly above the positive control. This relationship did not function in the reverse; substituting PTEC-Tert components for HUVEC-Tert components in PTEC-Tert base medium resulted in cellular death (figure 5c). The PTEC-Tert culture medium resulted in nearly complete HUVEC-Tert cellular death, while the PTEC-Tert base medium with added HUVEC-Tert components produced an enhanced cellular metabolic activity of approximately 20% greater than the positive control. This set of MTS assays supported the previous conclusion that PTEC-Tert components synergistically diminished HUVEC-

Tert viability. HUVEC-Tert culture medium components, conversely, did not individually or synergistically limit PTEC-Tert viability.

Since the PTEC-Tert culturing conditions threatened the HUVEC-Terts, an alternative vascular cell line was explored to determine whether PTEC-Tert media similarly affected it. RFP-GMECs were selected for their dual vascular and renal origins.

RFP-GMECs Exhibit Enhanced Tolerance of PTEC-Tert Media Relative to HUVEC-Terts

It was found that RFP-GMECs were less adversely affected by PTEC-Tert base medium with added GMEC components than were HUVEC-Terts cultured in PTEC-Tert base medium with added HUVEC-Tert components (figures 5c, 6a-b). Additionally, whereas the HUVEC-Terts were metabolically stressed in the 1:1 HUVEC-Tert to PTEC-Tert culture medium, the RFP-GMECs exhibited reduced viability in the analogous 1:1 GMEC to PTEC-Tert culture medium. Although cellular death was not desirable, it was preferable to the metabolic stress observed in the HUVEC-Tert plates because it was unknown whether the stress produced atypical HUVEC-Tert functional behavior or would ultimately induce cell death. These quantitative results were supported by light microscopy, which demonstrated that the RFP-GMEC morphology remained normal in the surviving and non-apoptotic cells compared to positive controls (data not shown).

In this initial set of MTS assays, the RFP-GMECs and PTEC-Terts were cultured separately from one another. However, in 3D-perfused culture, the exchange of media and secreted factors occurs mutually. The viability of the two cell types in co-culture with one another was thus assessed through MTS assays conducted in Transwell plates (figure 7) to permit interaction of the cultures through a semipermeable membrane. The RFP-GMEC viability was below 25% in all co-culture conditions with the PTEC-Terts, excluding the positive control (figure 7b). These values were approximately 5% lower than the negative control from the non-Transwell MTS assays (figure 6), but higher than values observed for HUVEC-Tert negative controls, which were between 5% and 20% cellular metabolic activity (figures 5a,c). The RFP-GMEC viability, when both wells were cultured in PTEC-Tert culture medium, was approximately equivalent to the viability when the RFP-GMEC insert well was cultured in RFP-GMEC culture medium (figure 7b), potentially implicating secreted PTEC-Tert factors in negatively affecting the RFP-GMECs. The PTEC-Tert cells survived at greater than 75% viability in all conditions except the negative control, in which their viability was reduced to approximately 40% (figure 7a). Collectively, the Transwell assays conducted on tissue culture plastic confirmed the deleterious and unidirectional effects of PTEC-Tert culture media and PTECs on vascular cell lines.

The chip-conditioned media did not significantly alter RFP-GMEC viability relative to PTEC-Tert culture medium. Figure 6 demonstrates approximately equal viabilities between RFP-GMECs cultured in PTEC-culture medium (G2a, G2b) and chip-conditioned PTEC-Tert culture medium (G8a), with viability lowered approximately 10% more in flask-conditioned PTEC-Tert culture medium (G8b). When RFP-GMEC components were added to chip-conditioned PTEC-Tert culture medium (G6a), the viability increased relative to chip-conditioned culture medium without GMEC components (G8a). When RFP-GMEC components were added to flask-conditioned PTEC-Tert culture medium (G6b), the viability did not significantly differ from flask-conditioned medium without GMEC components (G8b). The RFP-GMEC components did not appear to differently affect RFP-GMEC viability in flask-conditioned PTEC-Tert medium (G3a) compared to RFP-GMEC components in chip-conditioned medium (G6a).

a

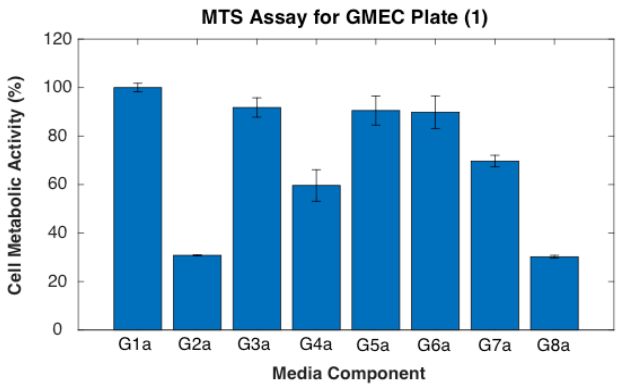

b

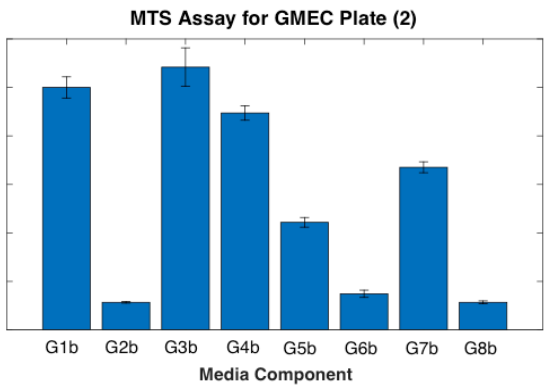

c

Media Conditions and Formulations

Condition	Formulation	Condition	Formulation
G1a	GMEC culture medium	**G1b**	GMEC culture medium
G2a	PTEC-Tert culture medium	**G2b**	PTEC-Tert culture medium
G3a	Conditioned PTEC culture medium (from flask) with added GMEC components	**G3b**	GMEC culture medium with 1% aprotinin
G4a	GMEC culture medium with 1% aprotonin	**G4b**	PTEC-Tert base medium with GMEC components
G5a	1:1 GMEC to conditioned PTEC-Tert culture medium (from chip)	**G5b**	1:1 GMEC to conditioned PTEC-Tert culture medium (from flask)
G6a	Conditioned PTEC-Tert culture medium (from chip) with added GMEC components	**G6b**	Conditioned PTEC-Tert culture medium (from flask) with GMEC components
G7a	1:1 GMEC to PTEC-Tert culture medium	**G7b**	1:1 GMEC to PTEC-Tert culture medium
G8a	Conditioned PTEC-Tert culture medium (from chip)	**G8b**	Conditioned PTEC-Tert culture medium (from flask)

Figure 6: RFP-GMECs exhibit enhanced viability in PTEC-Tert media relative to HUVEC-Terts. MTS assays were conducted for RFP-GMECs cultured in PTEC-Tert media formulations. Media formulations labeled in (a-b) are delineated in (c).

PTEC-Terts and Primary PTECs Yield Comparable Viabilities

Although it was necessary to incorporate proximal tubule epithelial cells into the proximal tubule channel to establish the greatest possible physiological relevancy, PTEC-Terts produced deleterious effects on the vascular cell line. A second proximal tubule cell line, the primary line, was investigated to determine whether it produced lower toxic effects than did PTEC-Terts. The Transwell co-culture experiments were replicated using primary PTECs in place of immortalized PTECs (figure 7). Overall, the Transwell MTS assays demonstrated that PTEC-Terts and primary PTECs survived relatively well in co-culture with the RFP-GMECs. In general, the PTEC-primaries demonstrated slightly greater viability in co-culture with the RFP-GMECs relative to PTEC-Terts (figure 7), a trend that was observed across all media conditions in the Transwell plates conducted using tissue culture plastic as the seeding substrate. However, the difference in viability was not statistically significant and did not provide sufficient motivation to replace the renal cell line in the vascularized PT model with PTEC-primaries. The viabilities of the PTEC-Tert and primary PTEC cells were relatively preserved across all conditions except the negative controls.

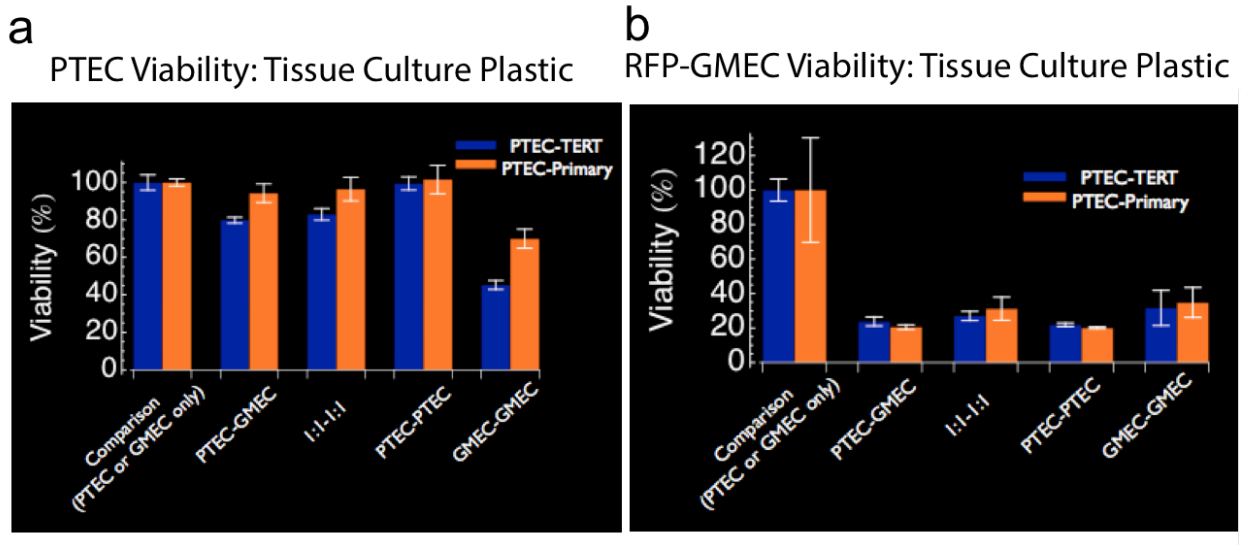

Figure 7: RFP-GMCs demonstrate slightly elevated viability in static co-culture with PTEC-Terts compared to HUVEC-Tert viability in independent culture. Figure (a) shows PTEC-Tert and primary PTEC viabilities. Figure (b) shows RFP-GMEC viabilities when co-cultured with PTEC-Terts or primary PTECs. These graphs were produced by Dr. Neil Lin using Mathematica.

Characterizing Cellular Expression and Morphology on the Extracellular Matrix

Since 2D, static viability assays demonstrated that RFP-GMECs posed a viable alternative to HUVEC-Terts when used as a vascular cell line in conjunction with PTEC-Terts, further experiments were performed to assess their behavior on various extracellular matrices and within

3D-perfused co-culture with PTEC-Terts. The following sections describe experiments aimed at evaluating the potential to integrate RFP-GMECs into the vascularized PT model alongside PTEC-Terts.

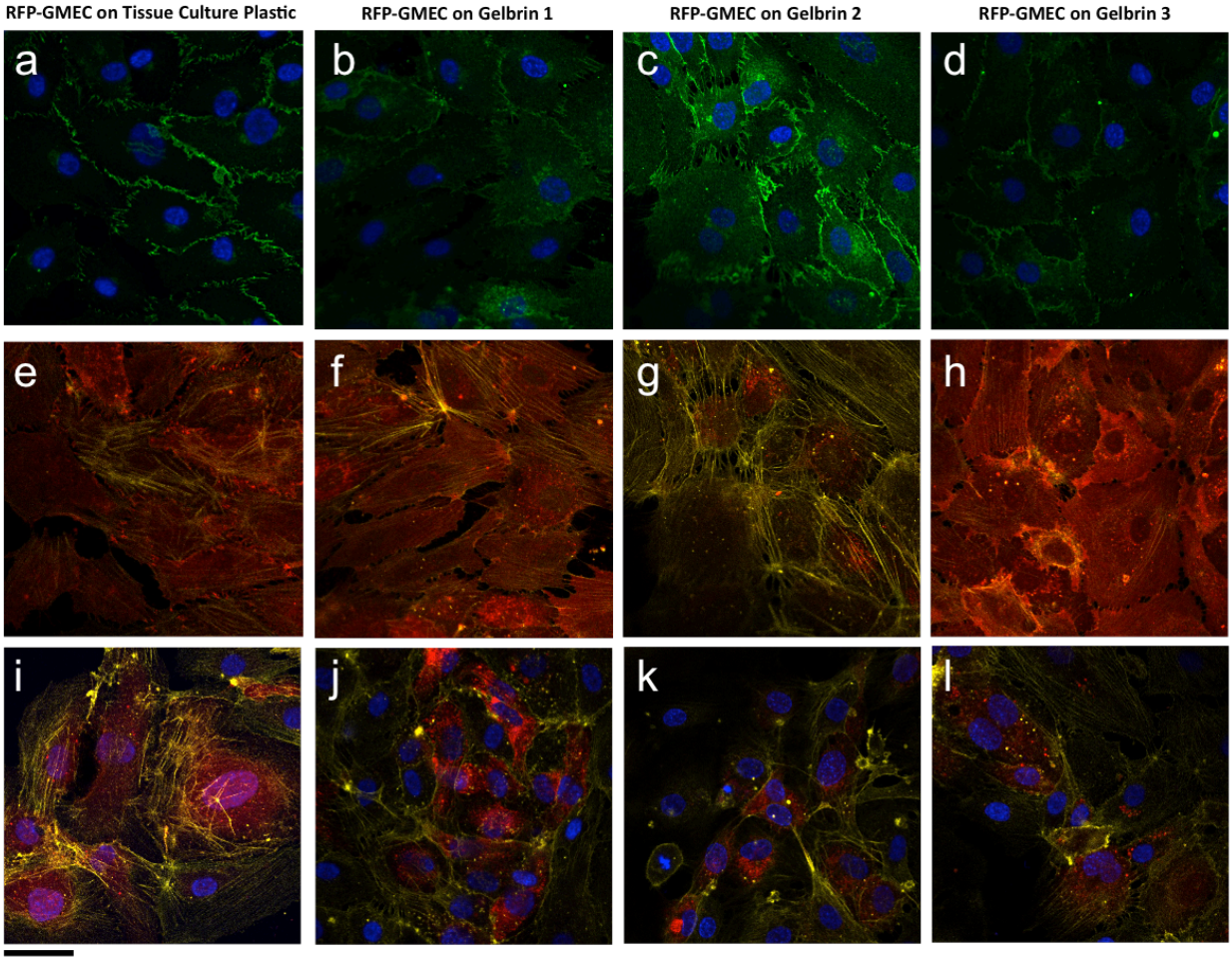

Figure 8: RFP-GMECs express vascular markers when cultured statically in 2D on extracellular matrix substrates. Each set of samples within an individual column pictured above was cultured on the substrate identified in the column heading. The cells depicted in (a-d) show stains for DAPI (blue) and $Na^+/K+$ ATPase (green). The cells depicted in (e-h) derived from the same cells in (a-d) and show stains for actin (yellow) and CD146 (red). The cells depicted in (i-l) derived from a second set of samples and show stains for DAPI (blue), actin (yellow), and CD31 (red). The images represent individual z-slices. The scale bar measures 50 μm.

RFP-GMECs and PTEC-Terts Show Characteristic Morphology on ECMs in 2D Culture

The previously published 3D-perfused proximal tubule model utilized an ECM formulation containing 7.5 wt% gelatin, 10 mg/mL fibrin, 0.2 wt% TG, and 2.5 mM $CaCl_2$ (Gelbrin 3) [9]. However, gelatin itself presents a less macroporous material than fibrin, obstructing diffusion through the extracellular matrix. Furthermore, PTECs were previously found to exhibit enhanced doming on hydrogels containing greater quantities of gelatin (data not shown). Doming is a

characteristic phenomenon in which PTEC monolayers elevate from a substrate in a circular fashion due to ion transport activities and accumulation of liquid under the 'dome' [18]. Doming presents the dangerous potential for PTEC monolayers to detach from the epithelialized channel. For this reason, extracellular matrix formulations consisting of lower gelatin concentrations were tested, and these have been described in the "Materials" section. Briefly, Gelbrin 1 contained 1 wt% gelatin, Gelbrin 2 contained 4.5 wt% gelatin, and Gelbrin 3 contained 7.5 wt% gelatin. Gelbrin 3 represented the previously reported ECM for the 3D-perfused PT [9]. A substrate consisting of tissue culture plastic without an ECM coating was introduced as a control. Individual z-slices are presented in figure 8 and combined maximum intensity projected z-stacks are shown in figure 9.

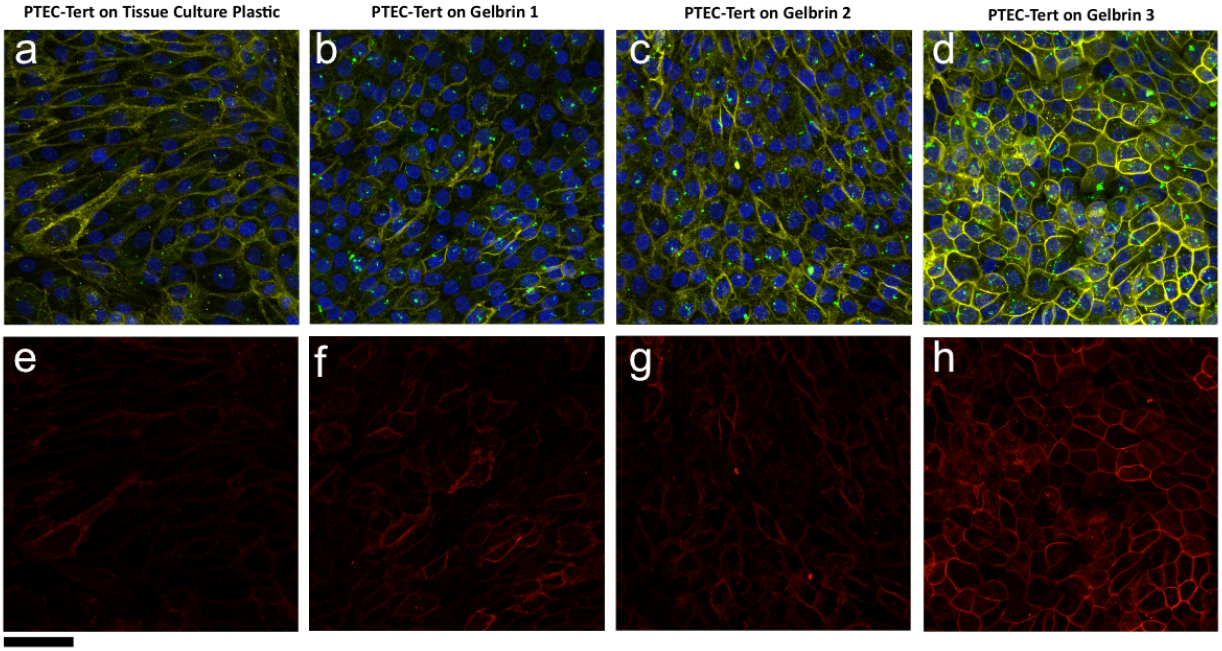

Figure 9: PTEC-Terts express renal markers when cultured statically in 2D on extracellular matrix substrates. Each set of samples within an individual column pictured above was cultured on the substrate identified in the column heading. The cells depicted in (a-d) show stains for DAPI (blue), actin (yellow), and acetylated tubulin (green). The cells depicted in (e-h) derived from the same cells in (a-d) and show a stain for Na^+/K^+ ATPase. The images represent combined maximum intensity projection z-stacks. The scale bar measures 50 μm

The RFP-GMECs appeared to express actin, Na^+/K^+ ATPase, and CD146 on all extracellular matrix formulations tested. The PTEC-Terts appeared to express actin and acetylated tubulin the strongest on Gelbrin 3 (figure 9), followed by Gelbrin 2. However, although not apparent from the upper images, the PTEC-Terts exhibited significant doming and subsequent detachment from the Gelbrin 3 matrix. The section imaged to produce figure 12 depicts one of the few adhered regions. The bottom panel of the Gelbrin 3 substrate provides a representative

indication of cellular density in one of the regions devoid of the PTEC-Tert monolayer. The monolayer adhered more completely to the Gelbrin 1 and Gelbrin 2 formulations, with some doming occurring on Gelbrin 2 (data not shown). For both cell types, the cell shapes and packing appeared to be healthiest by days 8 and 9 of culture on Gelbrin 1 (figure 10).

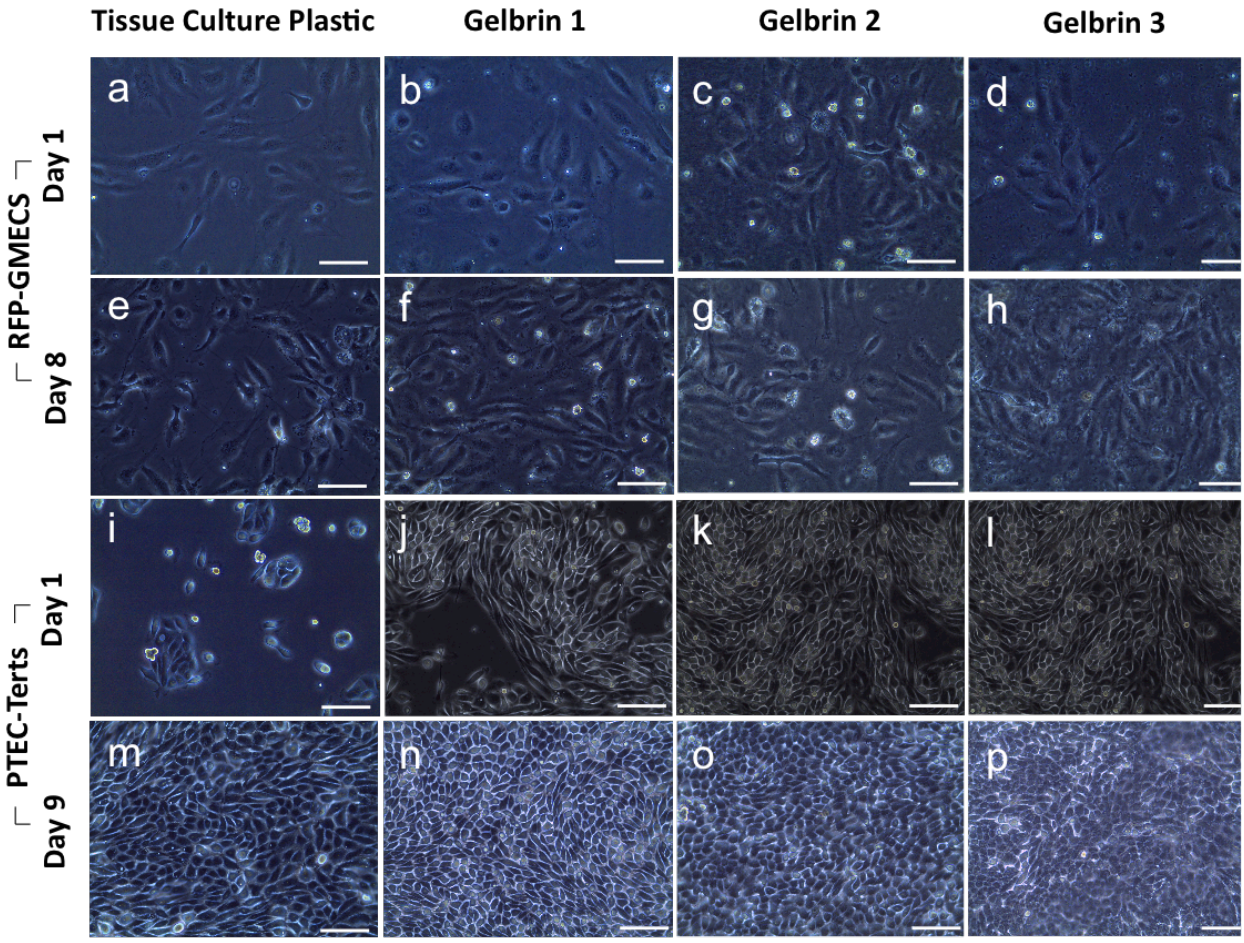

Figure 10: PTEC-Terts and RFP-GMECs exhibit healthiest morphology on Gelbrin 1 relative to controls. Figures (a-h) depict RFP-GMECs without an ECM substrate (a and e), on Gelbrin 1 (b and f), on Gelbrin 2 (c and g), and on Gelbrin 3 (d and h). Figures (i-p) show PTEC-Terts without an ECM substrate (i and m), on Gelbrin 1 (j and n), on Gelbrin 2 (k and o), and on Gelbrin 3 (l and p). All scale bars are 100 μm.

RFP-GMECs Express Appropriate Vascular Markers in 3D-Perfused Culture

The RFP-GMECs demonstrated expected morphology and marker expression in 3D-perfused co-culture with PTEC-Terts (figure 11). Specifically, platelet endothelial cell adhesion molecule, also called cluster of differentiation 31 (CD31), was identified throughout the cell body (figure 11b). Vascular endothelial cadherin (VE-cadherin) appeared to be enriched at the cell

membrane, demonstrating the tight cell-cell junctions (figure 11d) expected in vascular cell morphology.

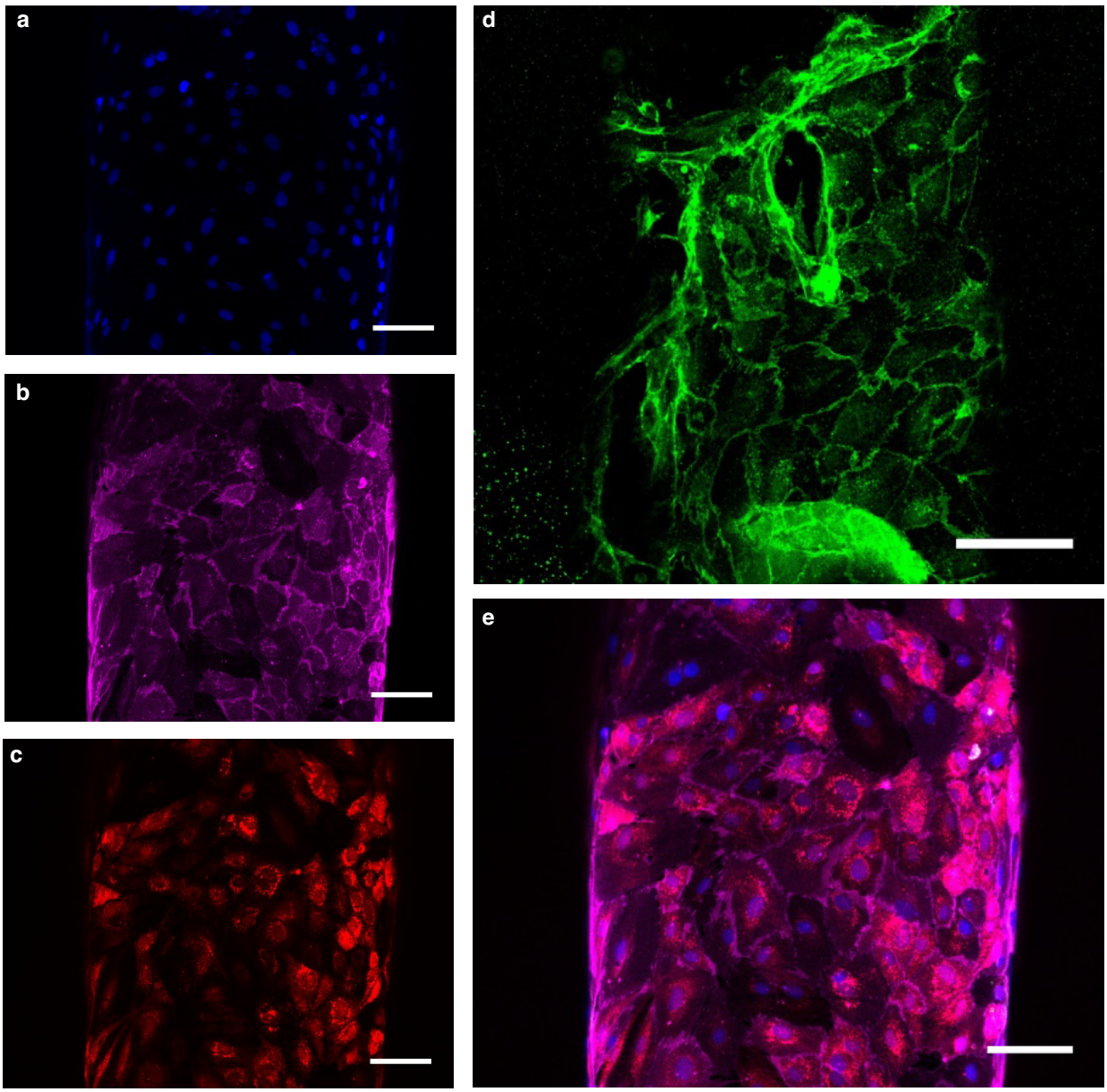

Figure 11: RFP-GMECs express appropriate vascular cell markers and phenotypic morphology in 3D perfused culture. RFP-GMECs were stained for (a) DAPI, (b) CD31, (c) RFP, and (d) VE-cadherin. A merged image of DAPI, CD31, and RFP appears in (e). The RFP-GMECs in these images were fixed and stained at day 5 post-seeding. All scale bars are 100 μm.

PTEC-Terts Express Appropriate Renal Markers in 3D-Perfused Culture

Similarly, the PTEC-Terts demonstrated expected renal morphology and marker expression in 3D-perfused co-culture with RFP-GMECs (figure 12). The PTEC-Terts expressed actin filaments (figure 12b) and a thickened epithelial lining (figure 12e) relative to the flat endothelial

monolayer (figure 12d). Na^+/K^+ ATPase was expressed basally and laterally along the cellular membrane in the PTECs (figure 12f).

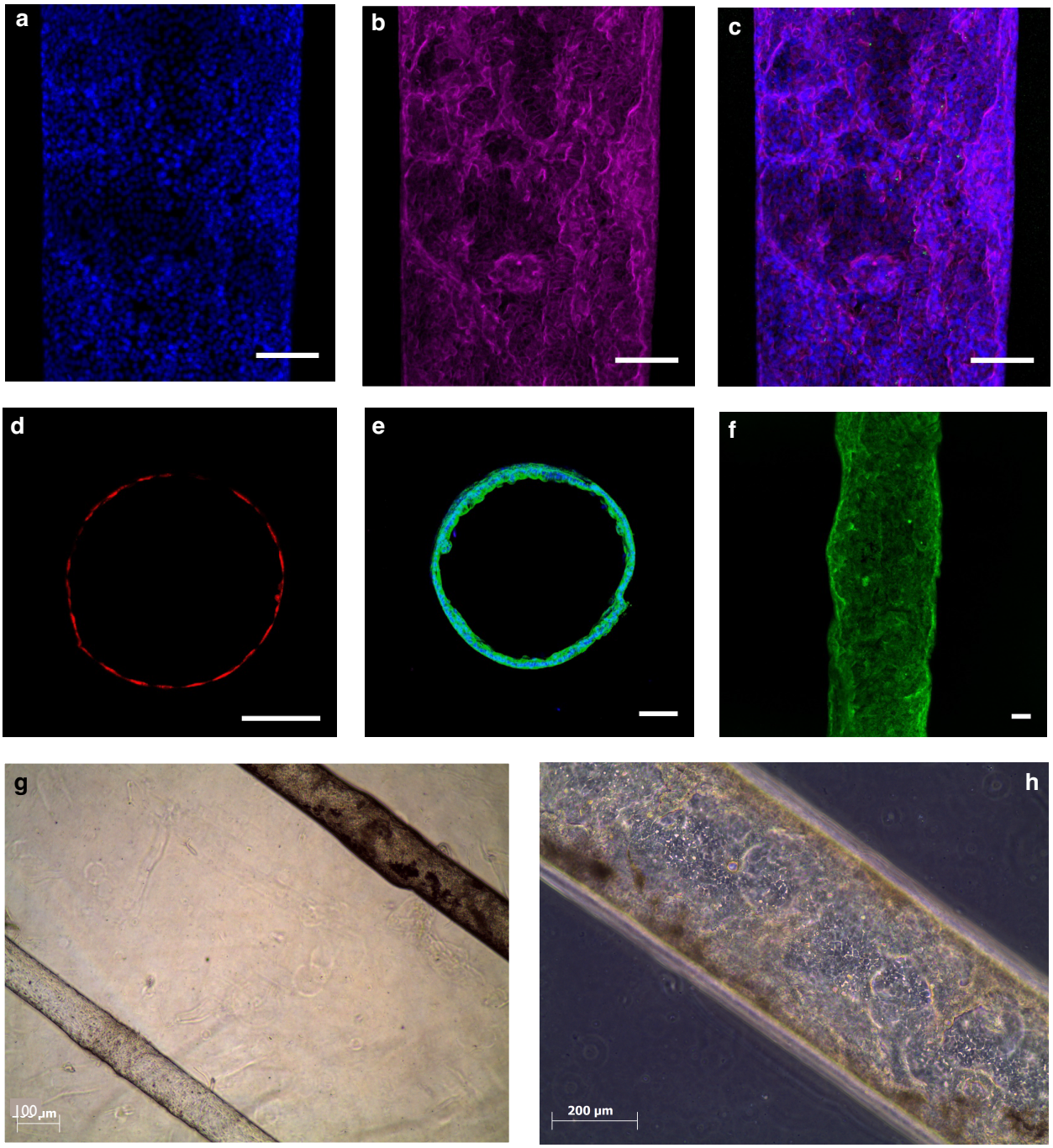

Figure 12: PTEC-Terts and RFP-GMECs express appropriate renal and vascular cell markers and phenotypic morphology in 3D perfused culture. PTEC-Terts were stained for (a) DAPI, (b) actin, (c) RFP, and (f) Na^+/K^+ ATPase. Figures (d) and (e) show tubular cross-sections in the same chip, with (d) representing the vascular line and (e) representing the PT. Figure (e) is a merged image of DAPI (blue) and Na^+/K^+ ATPase (green). The PTEC-Terts in (a, b, c, e, f) were fixed and stained at day 11 post-

seeding. The RFP-GMECs in (d) were fixed and stained at day 5 post-seeding and are shown alongside the PTEC-Terts in (e) to demonstrate height differences in the endothelial and epithelial layers. Figure (g) is a brightfield image of the adjacent PTEC-Tert and RFP-GMEC channels at day 10 and day 4 post-seeding, respectively. Figure (h) is a phase image of the PTEC-Tert channel at day 8 post-seeding. Scale bars are 100 μm in (a-g) and 200 μm in (h).

Additionally, the PTEC-Terts and RFP-GMECs were imaged via transmission electron microscopy (TEM) to determine whether they exhibited appropriate morphological features in 3D-perfused co-culture. Dr. Kimberly Homan and Dr. Neil Lin generously performed the imaging. On Gelbrin 1, the RFP-GMECs demonstrated small cellular heights (figure 13a) and characteristic intertwining tight junctions (figure 13c). The PTEC-Terts demonstrated microvilli lengths that measured approximately 2 μm on average (figure 13b).

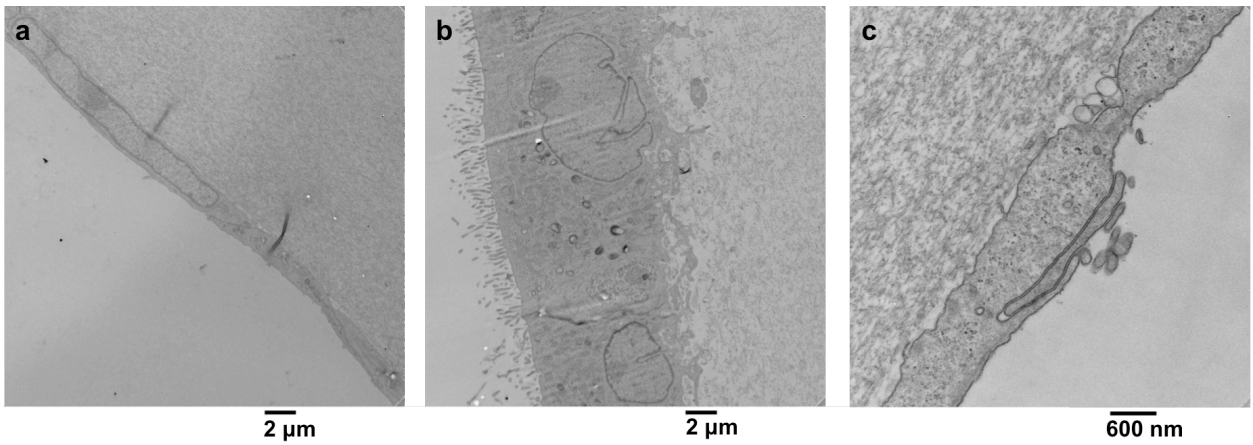

Figure 13: PTEC-Terts exhibit extended microvilli and RFP-GMECs demonstrate small cell heights along tight junctions in 3D-perfused culture within Gelbrin 1. The images depicted here were collected using transmission electron microscopy (TEM). Figure (a) depicts an endothelial cell cross-section. Figure (b) shows an epithelial cell cross-section with microvilli measuring approximately 2 μm in height. Figure (c) demonstrates a tight junction between endothelial cells.

The microvilli lengths reported in the previous 3D PT model were 1.4 μm on average on Gelbrin 3 (figure 14a) [9]. Since longer microvilli lengths enhance PTEC functionality by permitting greater extension into the lumen for reuptake of molecules from the glomerular filtrate, the microvilli length represented an aspect of improved physiological character on Gelbrin 1 relative to Gelbrin 3. The thickened PTEC-Tert cell height relative RFP-GMEC height demonstrated characteristic morphological differences between the two cell types. The height comparison was further visible in the confocal images, where the endothelial height (figure 12d) was smaller than the epithelial height (figure 12e).

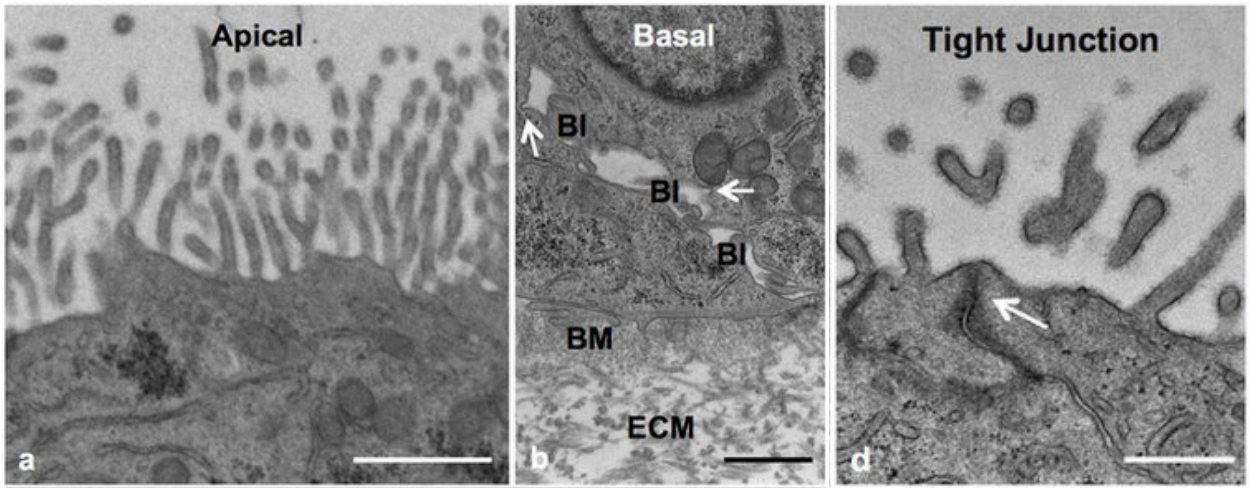

Figure 14: PTEC-Terts exhibit shorter microvilli and tight junctions in 3D-perfused culture with Gelbrin 3. This figure has been adapted from figure 3 of the work conducted by Homan *et al.* [9]. The scale bars in (a) and (b) measure 1 μ m, and the scale bar in (c) measures 10 μm. Figure (a) demonstrates microvilli forming an epithelial brush border. Figure (b) demonstrates Gelbrin ("ECM") and the basement membrane secreted locally by the cells ("BM"), as well as characteristic basolateral interdigitations ("BI"). Figure (c) depicts a tight junction between the epithelial cells.

Assessing Transepithelial Transport

PTEC-Terts Exhibit Transepithelial Transport of Locked-Nucleic Acid

The primary motivation for incorporating a vascular line into the proximal tubule model was to move towards establishing interaction between the proximal tubule and vasculature, which necessarily involves transepithelial transport by PTECs. To this end, an epithelialized channel was assessed for its capacity of transepithelial transport of locked-nucleic acid. The LNA uptake assay demonstrated successful transport when the LNA was delivered apically or basally to the PTEC-Terts (figure 15). There were no significantly observable differences in the uptake levels or character between apically and basally infused chips, with expected basal expression of Na^+/K^+ ATPase occurring in both of these chips to confirm standard PTEC-Tert behavior (figures 15f,h,j,l). The LNA itself appeared to be present throughout the cell body, with the exception of numerous "vacuoles" in which it seemed to be absent. Real-time imaging of basally delivered LNA demonstrated that LNA diffused uniformly out of the empty channel and into the proximal tubule line over the course of six hours (figure 15 b-e). The extracellular matrix therefore demonstrated sufficient permeability to allow diffusion of the LNA. The PTEC-Terts subsumed the LNA, demonstrating their potential to reabsorb nutrients delivered basally from a pseudo vascular line in the vascularized PT model as well as apically. The LNA that appears clustered within the empty channel has adhered to pieces of debris that populated the channel during fabrication.

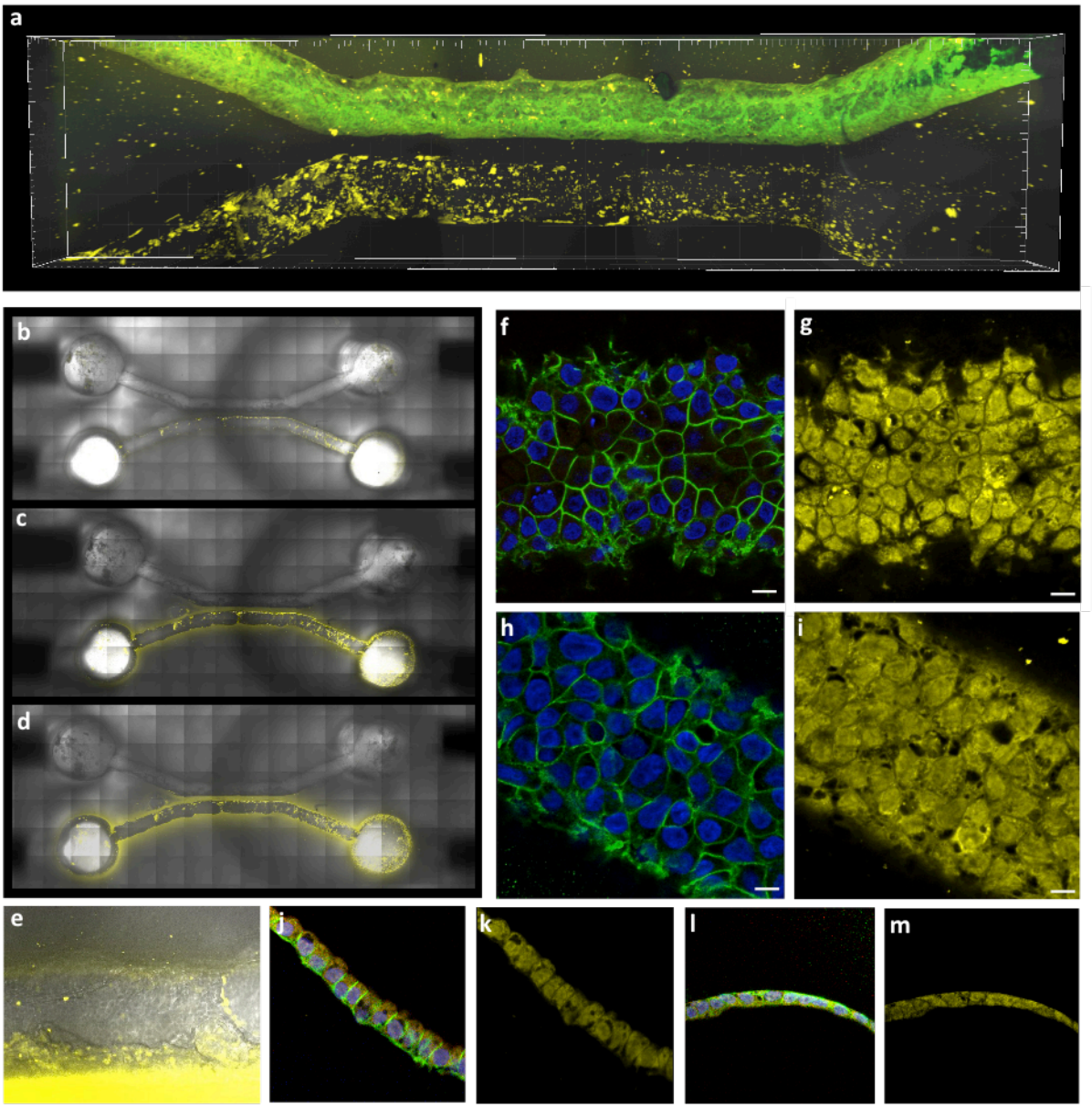

Figure 15: PTEC-Terts transepithelially transport locked-nucleic acid. Figure (a) shows the locked-nucleic acid disposition test for basal administration of the LNA. Figures (b-e) demonstrate a time lapse of a second test of LNA delivered basally to the PTEC-Terts, with images taken every two hours. The empty channel appears below the epithelialized channel, with some LNA adhering to gelbrin debris within the empty channel. Figures (b-d) chronologically depict a lapse of six hours from perfusion of the LNA, with figure b representing a lapse of two hours, figure (c) representing a lapse of four hours, and figure (d) representing a lapse of six hours. Figure (e) depicts a magnified view of the epithelial monolayer, demonstrating uptake of LNA by the PTEC-Terts from the extracellular matrix. Figures (f-m) demonstrate stains of Na^+/K^+ ATPase (green), DAPI (blue), and LNA (yellow) for LNA delivered basally (f, g, i, k) and apically (h, I, l, m). Scale bars measure 1 mm. Dr. Homan and Dr. Lin performed the perfusion and confocal imaging.

Seeding the Vascularized Proximal Tubule Model

PTEC-Terts and RFP-GMECs Survive for Three Weeks in 3D-Perfused Co-Culture

The vascularized proximal tubule model was ultimately seeded with PTEC-Terts in the proximal tubule channel and RFP-GMECs in the vascular channel within an extracellular matrix containing the Gelbrin 2 formulation. After three weeks, the two cell types had been in 3D-perfused co-culture with one another and were still viable (figure 16b).

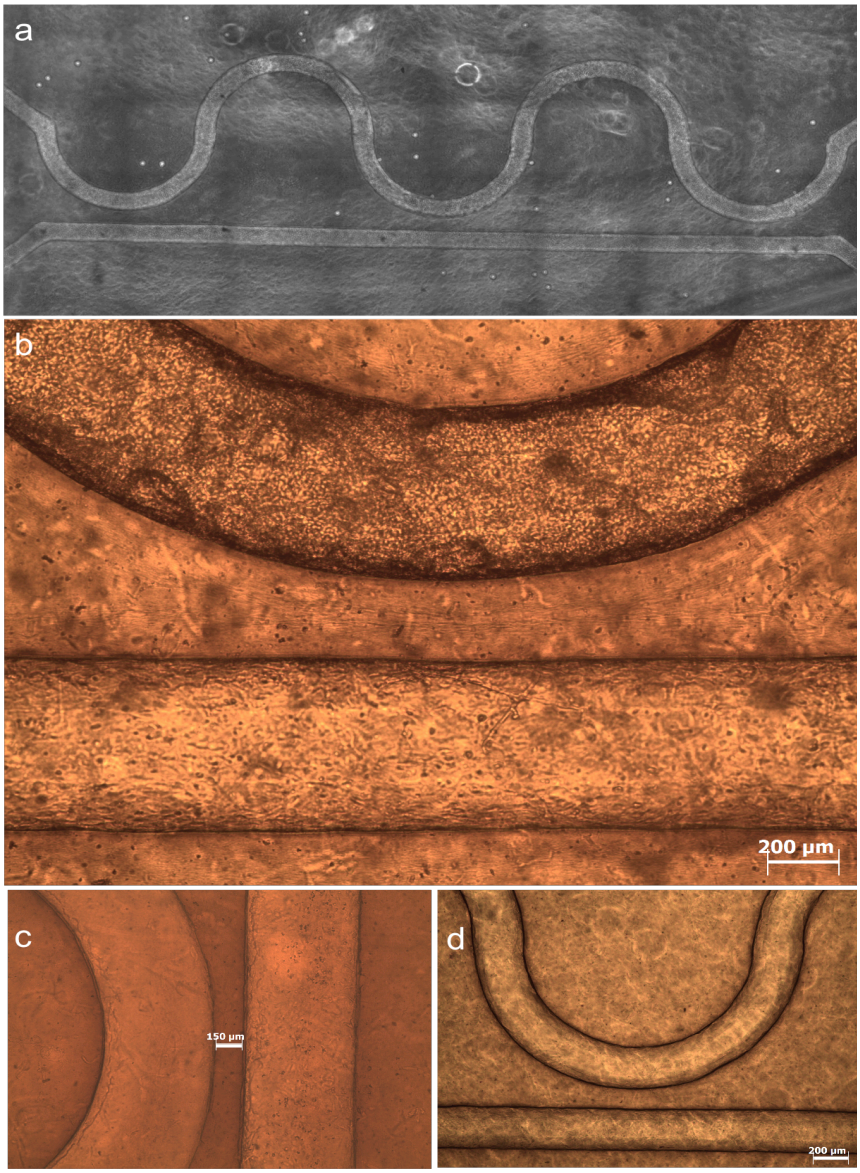

Figure 16: Bioprinted model of the 3D vascularized proximal tubule. Figure (a) depicts the entire vascularized model seeded with HUVEC-Terts and PTEC-Terts at 2.5X, one day before HUVEC-Tert cellular death was observed. Figure (b) demonstrates an epithelialized and endothelialized model at day 19 of co-culture. Figure (c) indicates an interstitial distance of approximately 150 µm separating the two channels of a bioprinted model. Figure (d) shows an alternative view of an acellular model.

V. Discussion

Vasculature provides the convoluted proximal tubule with an external source of nutrients and oxygen, as well as a means by which to secrete molecules reabsorbed from the glomerular filtrate into recirculation. Incorporating a blood vessel surrogate into the 3D perfused PT expands the tubule's physiological relevance by providing an opportunity to recapitulate these *in vivo* functions. The vascularized proximal tubule model was designed to minimize the interstitial distance between the proximal tubule and the vascular line to permit these physiological interactions. Since most cells in the body are positioned within 100 – 200 μm of capillaries to overcome diffusional limitations on oxygen [19], it was necessary to constrain this distance within 200 μm to permit diffusion of oxygen, nutrients, and waste products across the extracellular matrix. As demonstrated by the locked-nucleic acid transport study, a separation distance of under 200 μm permitted diffusion of nucleic acid from the proximal tubule to the pseudo vascular line on relevant timescales. Iterations of the final model demonstrated in figure 16 contained separation distances between 100 and 250 μm.

A second design consideration was the geometry of the proximal tubule line. In printing the vascularized model, a sinusoid wave was invoked to represent the proximal tubule. The sinusoid was selected because it provided regions of proximity to the vascular line for analyzing transport between the tubes, as well as regions of greater interstitial distance to enable future studies of the effect of distance from the vascular line on PTEC-Tert or GMEC behavior. The symmetry of the sinusoid further provided technical replicates to enhance statistical analysis in the form of three peaks and three troughs. The curvature of the sinusoid echoed the convolution incorporated into the non-vascularized 3D perfused PT constructed by Homan *et al* [9].

Initial seeding of the vascularized PT model was conducted using HUVEC-Terts because previous work in the Lewis Laboratory focused on generating 3D vascularized thick tissue with HUVECs as the vascular cell line [8]. It was found that HUVEC-Terts died by day four of 3D-perfused co-culture with PTEC-Terts. Although it is possible that contamination caused cellular death, an alternative antagonist was identified as media incompatibility between the two different cell lines. In 3D, PTEC-Tert medium components access the HUVEC-Tert cells by diffusing from the PTEC-Tert medium into the channel containing HUVEC-Terts. The components then interact with the HUVEC-Tert culture medium being perfused through that channel. Relative to previous constructs incorporating PTEC-Terts and HUVEC-Terts, the proximity of the proximal tubule line

to the vascular line minimized the distance across which PTEC-Tert media diffused to ultimately enter the vascular line, potentially leading to rapid cellular death.

A series of subsequent MTS assays demonstrated support for this hypothesis (figure 5). These MTS assays were designed to analyze HUVEC-Tert and PTEC-Tert viability when cultured in components of one another's media. Individual components were tested discretely to distinguish single-component effects from synergistic effects of combining the components into a single medium formulation. The components were added directly to culture medium, rather than base medium, because standard culture medium was used in the 3D-perfused environment. Overall, it was determined that synergistic effects produced by interactions of the entire set of media supplements were responsible for the cellular death observed in HUVEC-Tert culture. The base medium itself appeared to place the HUVEC-Terts under metabolic stress, but did not produce widespread apoptosis (figures 5a,c). Regardless, since PTEC-Tert media supplements are essential to PTEC-Tert viability and morphology, it would be impossible to remove these components from the media used to perfuse the renal line of the vascularized PT model. It became necessary to identify an alternative vascular line that could withstand potential cytotoxic effects produced by the PTEC-Tert culture medium. Interestingly, Miya *et al.* demonstrated stimulation of PTECs by matrix metalloproteinases secreted by human umbilical vein endothelial cells (HUVECs), the two cell types initially explored in this thesis, in nested culturing wells separated by a porous membrane to permit diffusion between the wells [20]. It is possible that the different culture media utilized by this laboratory did not initiate the same cytotoxic events observed in our system. It is further possible that the HUVEC-Terts tested in our laboratory originated from an unhealthy supply. Assays were conducted to understand the source of cell death within the perfused model as well as to explore alternative vascular lines that exhibited enhanced viability relative to immortalized HUVECs.

A second series of MTS assays was conducted to analyze whether glomerular microvascular endothelial cells, or GMECs, could provide an alternative to HUVEC-Terts in the vascularized model. GMECs possessed the biomimetic advantage of originating from the glomerulus, the filtration unit in the kidney that is encapsulated within Bowman's capsule and precedes the proximal convoluted tubule. The GMECs utilized in the MTS assays were labeled with red fluorescent protein (RFP) to assist with visualization through fluorescent light microscopy. The MTS assays performed in standard culturing plates demonstrated that RFP-GMECs survived moderately well in PTEC-Tert culture medium and conditioned PTEC-Tert medium (figure 6). The conditioned medium was introduced to permit analysis of the effects of factors secreted exogenously by the

PTEC-Terts on the RFP-GMECs. It was found that RFP-GMEC viability was approximately equal at a low level when cultured in conditioned PTEC-Tert culture medium compared to unconditioned PTEC-Tert culture medium for both chip-conditioned (figure 6a) and flask-conditioned (figure 6b) media, demonstrating a lack of support for our hypothesis that conditioned media contained fewer PTEC-Tert supplemental media components than did culture media due to uptake of the components by the cultured cells. However, conflicting data was demonstrated by results that suggested RFP-GMEC components did not increase viability in flask-conditioned media relative to RFP-GMEC components chip-conditioned media, despite an increase in viability within the MTS assay incorporating chip-conditioned medium (G6a vs G8a) and a lack of increase in flask-conditioned medium (G6b vs. G8b). These studies can be possibly attributed to batch variations in the conditioned medium and the MTS assay, and will need to be repeated for further analysis. In all cases, conditioned or unconditioned PTEC-Tert culture medium without RFP-GMEC components lowered RFP-GMEC viability to between 10% and 30% from the positive control.

It was further determined that flask-conditioned PTEC-Tert culture medium lowered RFP-GMEC viability by approximately 20% more than did chip-conditioned PTEC-Tert culture medium (figure 6). The secreted factors may have varied between the "flask" and "chip" sources for two primary reasons. First, the cells in the flask were exposed to static medium, while the cells in the chip experienced shear stress from the flowing medium. The difference in mechanical stimulation may have affected their secretory behaviors. Second, the surface area of the cellular culture in the flask was much larger than the surface area of the cellular monolayer in the chip, potentially increasing the concentration of secreted factors in the "flask" conditioned medium relative to the "chip" conditioned medium. The secreted factors present in the conditioned media from the chip provided a closer approximation of the levels at which they would be found in 3D-perfused culture than did the conditioned medium from the flask. Consequently, the RFP-GMECs demonstrated the potential to survive in 3D perfused co-culture with the PTEC-Terts.

Since the MTS assays were conducted on the renal and vascular cells in isolation, Transwell experiments were introduced to study cellular viability when the cells were co-cultured. It was found in Transwell culturing plates that, despite poor viability in co-culture with the PTEC-Terts (figure 7b), RFP-GMECs exhibited enhanced durability relative to HUVEC-Terts. Critically, the Transwell membrane permeability differs from the ECM hydrogel permeability, permitting rapid mixing of the two culture media if the endothelial layer is not tightly formed. The Transwell insert wells also have open sides that are exposed to the bottom wells, potentially permitting the 500 μL of medium in the

bottom well to dilute the 150 μL of medium in the insert wells. These circumstances of the Transwell plates may have contributed to the enhanced RFP-GMEC death observed in the Transwell MTS assays (figure 7).

The MTS offers an efficient surrogate assay for predicting cellular responses in 3D cultures using 2D culturing environments. However, the assay is sensitive to small discrepancies in volumetric media differences and cellular densities within the measured wells, making it prone to variability across instantiations. Future studies could therefore incorporate flow cytometry as a second method by which to measure cellular viability. In the context of this thesis, the MTS assay results were interpreted as indications that RFP-GMECs would survive longer and thrive better in 3D-perfused co-culture with PTEC-Terts than did the HUVEC-Terts. Thus, the MTS assays motivated the study and characterization of cellular behavior, morphology, and functionality in 3D-perfused co-cultures of RFP-GMECs and PTEC-Terts.

Chips were subsequently constructed to confirm that the RFP-GMECs expressed appropriate renal cell markers in 3D-perfused co-culture with PTEC-Terts. It was necessary to characterize their expression under these conditions because our laboratory had not used GMECs alongside PTEC-Terts before. It was found that RFP-GMECs expressed appropriate vascular markers and the PTEC-Terts expressed expected renal markers on Gelbrin 1, supporting the potential to use RFP-GMECs successfully in the 3D perfused vascularized proximal tubule model. Additionally, the microvilli length displayed by PTEC-Terts was increased on Gelbrin 1 relative to Gelbrin 3 (figures 13b,14a). Although the characteristic markers were expressed well on Gelbrin 1, the hydrogel possessed significant osmotic pressure differences with the Pluronic F127 fugitive bioink that destroyed the integrity of 3D printed channels (data not shown) and only permitted generation of the immunostained channels via the pin-pullout method.

The incompatibility of Gelbrin 1 with 3D bioprinting led to pursuit of alternative extracellular matrix formulations that could be interfaced with Pluronic F127. The morphological features and marker expressions were visualized for RFP-GMECs and PTEC-Terts cultured statically in 2D on varying ECM formulations. The purpose of this study was to determine whether Gelbrin 2, which offset osmotic pressure differences through increased gelatin and fibrin concentrations, achieved the same or improved morphology and expression relative to Gelbrin 1 and the previously reported Gelbrin 3 [9]. The morphology appeared to be healthiest on Gelbrin 1 (figure 10), but holistic marker expression for PTEC-Terts appeared to be favorable on Gelbrin 2 and Gelbrin 3 (figure 9). Since the doming and high gelatin concentration motivated selection

against Gelbrin 3 as the ECM for the vascularized proximal tubule model, Gelbrin 2 was selected as to form the extracellular matrix in the vascularized 3D PT model.

The PTEC-Terts demonstrated transepithelial transport when exposed basally and apically to LNA on Gelbrin 2. When delivered basally, the nucleic acid successfully diffused through the extracellular matrix prior to entering the proximal tubule channel. Functional assays to demonstrate interaction between endothelialized and epithelialized channels will be probed next. An immediate step following this thesis involves examining transport of fluorescently labeled human serum albumin (HSA) across the epithelial monolayer and into the basally located channel. Since PTECs reuptake albumin *in vivo*, it is hypothesized that the PTECs will reabsorb the HSA from the perfusing media, simulating the glomerular filtrate, and push it to the adjacent endothelialized vessel. Alternative perfused models have demonstrated successful reabsorption of HSA within an epithelialized tubule (see [9] and supplementary information). However, interaction with the blood vessel would demonstrate enhanced biomimetic functionality and successful vascularization of the construct.

The next iterations of the vascular design will likely resemble figures 4c and 4d. In the design represented in figure 4d, the vascular line has been brought into closer proximity to the entire proximal tubule line to enable molecular transport to the vessel at all sites along the tubule. Eventually, future work will involve embedding a printed vascular line within the proximal tubule geometry described by Homan *et al.* From a manufacturing standpoint, the G-Code generation process would enable dynamic adaptation of the vasculature to varying proximal tubule geometries. Printing the vascular line within this model would necessitate the introduction of z-axial directionality to span the tubules as depicted in figure 4d. The laboratory has conducted preliminary work to define such a feature using MeCode, a Python-based software suite for generating custom G-Code developed by Jack Minardi. However, specific design challenges remain, including the need for a bioink that maintains its fidelity when suspended in midair between two anchoring points printed on either side of the proximal tubule. The diameter of the printed bioink must also be reduced in order to print the vascular line in greater proximity to the proximal tubule and give the PT a more biomimetic diameter.

The experiments conducted in the course of this thesis demonstrate the development of a preliminary model of a vascularized convoluted proximal tubule constructed via 3D bioprinting. The channel simulating the blood vessel was endothelialized with glomerular microvascular endothelial cells, which exhibited greater longevity and renal character than the immortalized human

umbilical vein endothelial cells previously utilized as the vascular cell line. The proximal tubule was epithelialized with immortalized human proximal tubule epithelial cells, which populate the proximal tubule *in vivo* to reabsorb nutrients from the glomerular filtrate and pump them into the bloodstream. The PTEC-Terts demonstrated active transport within the 3D perfused model through transportation of apically and basally delivered LNA across the epithelial lining. The model presented here demonstrated successful 3D perfused co-culture of RFP-GMECs and PTECs for three weeks, with the culture ongoing at the time of submission.

VI. Conclusion

Multiple features of the vascularized 3D PT model presented here offer improved physiological relevance relative to previously reported proximal tubule models. Like the microfluidic chip developed by Jang *et al.*, the model positions a secondary channel within 200 μm of the proximal tubule to permit diffusion of macromolecules across the epithelial barrier. However, unlike the microfluidic PT, the model explored here endothelializes the secondary channel to simulate a blood vessel. Additionally, the model embeds both channels directly within a complex extracellular matrix, rather than limiting exposure to only one side of a 2D membrane coated in a single ECM protein [12]. The microphysiological system published by Weber *et al.* similarly contains two channels circumscribed by an encompassing 3D extracellular matrix. However, the MPS does not endothelialize the second tube to model vasculature or associated transport [14].

In the future, the vascularized 3D PT model will be expanded to incorporate vasculature into the preexisting 3D perfused PT geometry (figures 1a, 4d). The bioprinting approach demonstrated here will permit juxtaposition of vasculature with the convoluted geometry in multiple dimensions. Bioprinting also enables dynamic repositioning of the vascular and proximal tubule lines during the fabrication process, as well as rapid prototyping of numerous geometries. The pin-pullout and mold-based manufacturing techniques employed to produce previously reported microfluidic chips have limited potential to produce such architectures. Ultimately, the bioinks could be cellularized as previously demonstrated [8] to directly co-print the proximal tubule and vasculature without the need for seeding. The model presented in this thesis represents the first step towards generating such a 3D bioprinted vascularized convoluted proximal tubule for pharmacological and medical application.

VII. Supplementary Information

Analyzing the Role of Curvature Within the Convoluted Proximal Tubule

It was observed from analysis of an HSA uptake assay performed in the previously reported 3D PT that HSA may have been preferentially absorbed in regions of tighter curvature (data not shown), and it was hypothesized that this phenomenon potentially occurred due to fluid mixing and longer HSA residency times within the curved regions. If supported, the hypothesis may have contributed to functional understanding of why the proximal tubule exhibits convolution *in vivo*.

A model was generated to examine whether the macroscopic curvature of a channel lined with PTEC-Terts differentially affected PTEC-Tert uptake of human serum albumin (HSA), a molecule that the proximal tubule reabsorbs from the glomerular filtrate *in vivo*. The tubule geometry was designed to permit testing of three different degrees of curvature corresponding to arcs with three different radii. In the associated MATLAB file to generate G-Code for printing the curvature model, each of the three radii can be adjusted. The path contained a vertical line of symmetry to produce two technical replicates of each curvature angle within a single chip (Figure S1b). This model was printed, seeded with PTEC-Terts, and subjected to a human serum albumin (HSA) uptake assay.

The chip was printed using the design depicted in figures S1a-b and encapsulated in an extracellular matrix containing 7.5 w.t.% gelatin, 10 mg/mL fibrin, and 1 unit/mL thrombin. The chip was seeded with PTECs 25 days prior to performance of the HSA uptake assay. To conduct the assay, Cy3-labeled human serum albumin was perfused through the tubule at 50 μg/mL for three hours. The chip was then fixed in formalin and washed three times with PBS containing Ca^{2+} and Mg^{2+}. The chip was blocked prior to imaging on the confocal microscope.

It was observed that HSA was not preferentially taken up by the PTECs lining the tighter curves of the curvature model (Figure S1d-e). COMSOL modeling of flow within the printed curvature model further demonstrated laminar flow throughout the tubule (data not shown), suggesting that HSA did not experience differential residency times due to fluid mixing. It is possible that the tubule was not narrow enough to motivate increased PTEC-Tert packing densities within regions of greater curvature, or that the curves themselves were not tight enough to prompt differential uptake behavior. Future iterations of the model could be printed at smaller tubule diameters and with greater degrees of curvature to more fully investigate the role of convolution in determining PTEC behavior.

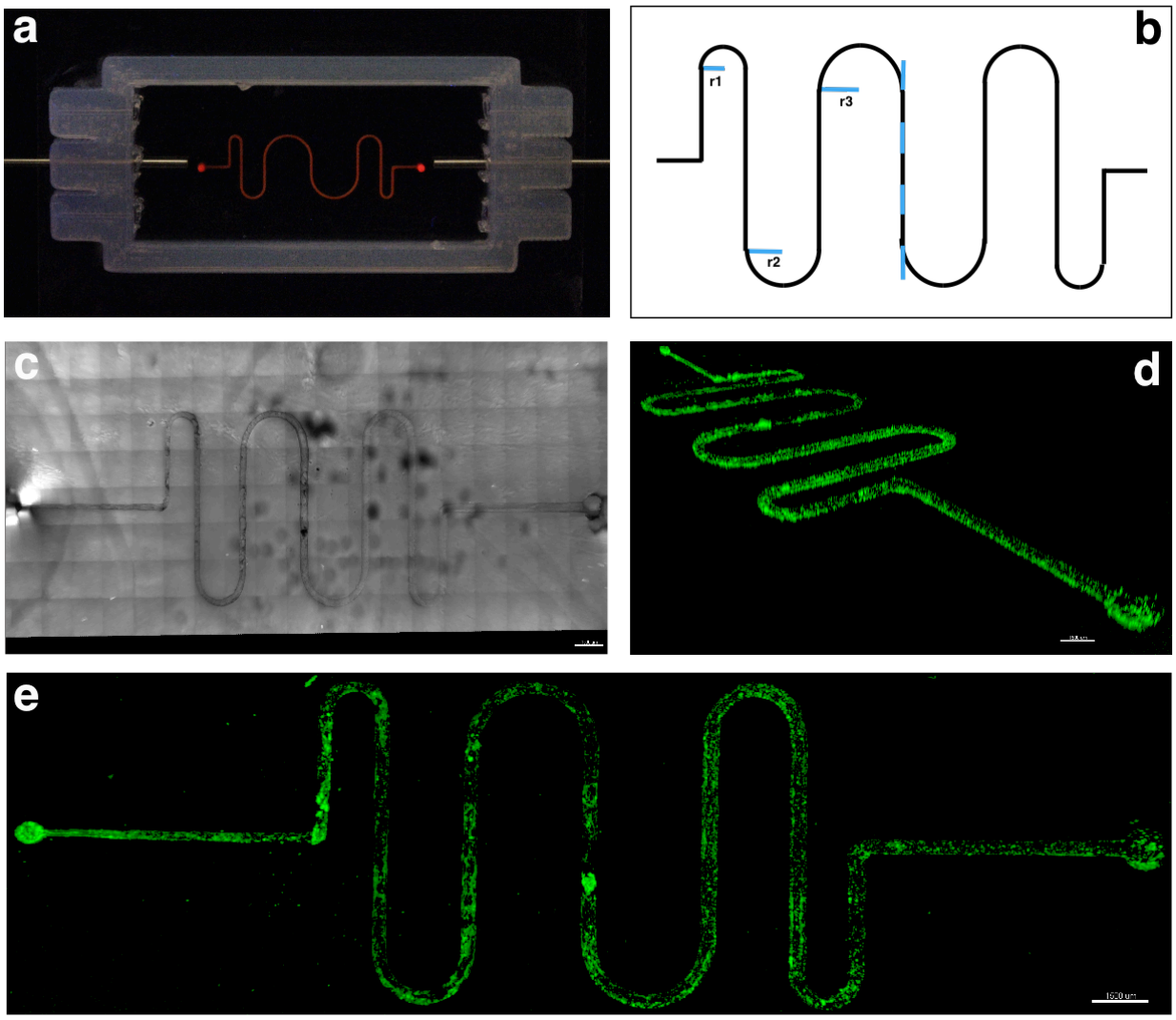

Figure S1: Curvature does not increase human serum albumin uptake by PTECs. Figure (a) is an image of the curvature model printed directly on a glass substrate using fluorescent Pluronic F127 ink. Figure (b) indicates the line of symmetry and differential radii of curvature. Figure (c) shows an image of the cellular deposition within the tubule structure. Figures (d) and (e) show the Cy3-labeled HSA within the tubule under confocal microscopy. The scale bars measures 1500 μm.

Minimizing the Diameter of the Proximal Tubule: Pin Pullout Using Glass Capillaries

Smaller tubule diameters better recapitulate the *in vivo* proximal tubule geometry. In this thesis, bioprinted features were limited to a minimum diameter of 100 μm. This was due to the diameter of the print nozzle itself, which was 50 μm in the smallest available diameter, and the swelling ratio of Pluronic ink when submerged in gelbrin, which was approximately 2X. The non-vascularized 3D PT model that we previously generated had diameters ranging from 400 to 550 μm [9]. For the 3D-perfused PTEC-Tert and RFP-GMEC expression studies described previously, the

tubule diameters were formed at 300 μm. This width represents the smallest diameter metal tubes that were available for use with the pin pullout method.

To develop channels with diameters smaller than 100 μm, the pin pullout method was employed using glass capillary tubes (figure S2). The inner tubes consisted of glass capillaries that had been pulled to diameters of 50 – 100 μm at the center. The glass capillary tubes were inserted into outer tubes, which had an outer diameter of 800 μm, and subjected to the same extracellular matrix casting procedures as before. The glass capillary tubes were later removed from the processed extracellular matrix in two ways. In the first method, they were carefully twisted to induce breakage at the center, which was the weakest structural point of the tube, and then removed from either end of the chip. In the second method, the entire glass capillary tube was carefully pulled through one side of the chip without breaking it.

While feasible within the context of this thesis, producing small diameters via glass capillary tube pullout does not present a sustainable fabrication option for large-scale production of perfusable chips. The glass capillary tubes themselves were fragile and extremely prone to breaking, particularly after they had been drawn to diameters of less than 100 μm. Many tubes broke while threading the glass capillary tubes through the outer metal tubes used in the pin-pullout technique. After the chips had been created, removing the glass capillaries from the extracellular matrix also presented challenges. It was found that breaking the glass at its narrowest width produced microscopic fragments that remained within the channel, compromising structural integrity. The most reliable approach to removing the glass entailed pulling it entirely through the outer pins without breaking it. However, this technique resulted in an unavoidable expansion of the channel's diameter as the undrawn parts of the glass passed through the narrowest segment. After the gelbrin decompressed, the channel diameter had expanded to approximately 100 μm in its narrowest section. Additionally, the small diameter of the channel itself produced large pressure differences that made it difficult to seed the channel with cells from a pipette tip. Cells ultimately could not be forced into the narrowest part of the channel and instead could only be seeded at the inlet and outlet. The high inner-channel pressure meant that the cells themselves were highly sensitive to slight fluctuations in pressure release at the tube openings, which occurred during media changes.

In the future, it would be preferable to print features at the required size using Pluronic F127 ink directly. Future work could involve titrating Pluronic at different weight percentages alongside different gelbrin formulations to offset the osmotic differences and reduce the Pluronic swelling ratio. Identification of an ink-matrix combination that permits high-fidelity printing without

swelling would permit greater print resolution. Using the print nozzles currently available to our laboratory, this would enable printing of channels at 100 μm in diameter. Smaller nozzles could be purchased to explore printing at diameters below 100 μm. However, great attention will need to be focused on avoiding drying of the inks at such small diameters during printing and methods of seeding the channels at such dimensions.

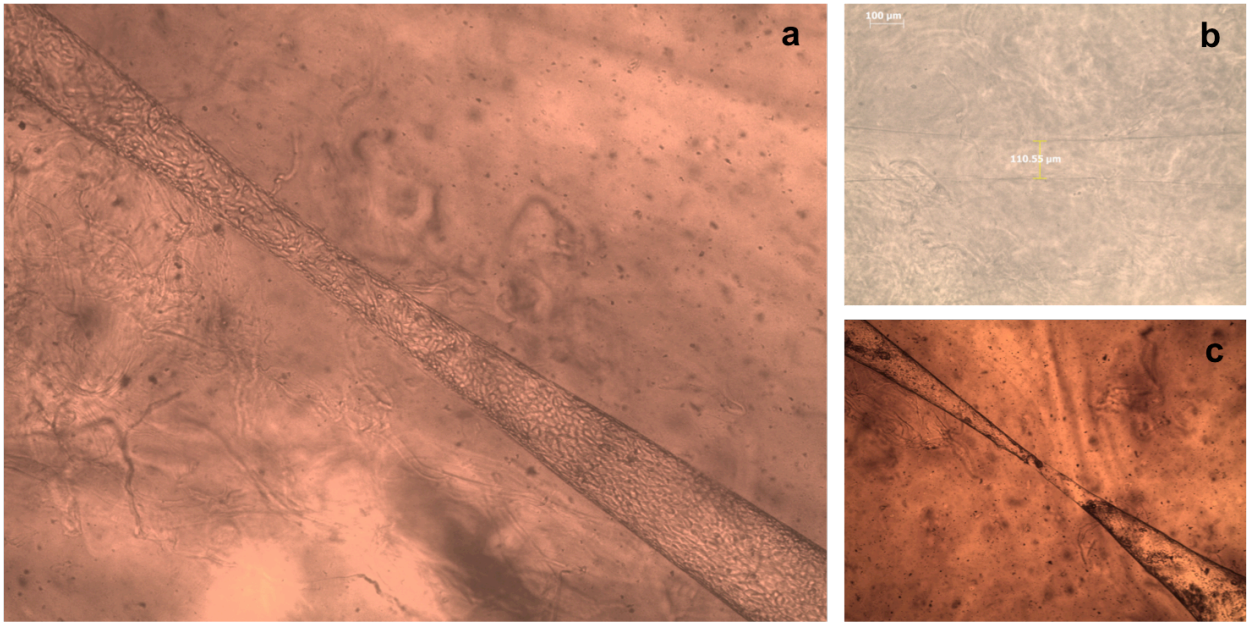

Figure S2: Epithelialized channels developed via glass pin-pullout. Figures (a) and (c) demonstrate channels 14 days and 12 days after seeding, respectively. Figure (b) demonstrates an empty channel with a measured width of approximately 100 μm.

VIII. Acknowledgments

I would like to thank numerous mentors, educators, and friends who assisted me in the course of researching and composing this thesis.

First, thank you to my principal investigator and professor, Dr. Jennifer Lewis, for generously permitting me to conduct research in her laboratory for the past two years. My time in the Lewis Lab has been among the most valuable of my engineering education, and I am grateful for the opportunity to have fostered my scientific skills through participation in projects, discussions, and friendships within the Lewis Lab community.

Next, I would like to extend my enormous gratitude to my wonderful research and thesis mentors, Dr. Kimberly Homan and Katharina Kroll, whose guidance has been fundamental to my development as an informed bioengineer. In particular, thank you to Kim for nurturing my passion for scientific inquiry and to Kathi for her responsiveness and patience teaching me crucial engineering skills.

I would like to sincerely thank other members of the renal tissue bioprinting team, Dr. David Kolesky, Dr. Neil Lin, and Dr. Annie Moisan, for insightful conversations, academic partnership, and camaraderie throughout this project. I would also like to thank other members of the Lewis Lab, including Dr. Mark Skylar-Scott, Dr. Sebastian Uzel, Donald Mau, and Dr. Scott Slimmer for their help and constant willingness to teach me.

Thank you to Dr. Linsey Moyer for her excellent academic guidance throughout my senior year at SEAS and for her kind willingness to read my thesis.

Finally, thank you to my supportive family and friends, especially to my parents, for constantly surrounding me with a network of encouragement and motivating conversations.

IX. References

1. Moon, K.H., et al., *Kidney diseases and tissue engineering.* Methods, 2016. **99**: p. 112-9.
2. System, U.S.R.D., *2016 USRDS annual data report: Epidemiology of kidney disease in the United States.* . 2016, National Institutes of Health, National Institute of Diabetes and Digestive and Kidney Diseases: Bethesda, MD.
3. Tiong, H.Y., et al., *Drug-induced nephrotoxicity: clinical impact and preclinical in vitro models.* Mol Pharm, 2014. **11**(7): p. 1933-48.
4. Chevalier, R.L., *The proximal tubule is the primary target of injury and progression of kidney disease: role of the glomerulotubular junction.* Am J Physiol Renal Physiol, 2016. **311**(1): p. F145-61.
5. Lindop, G.B., et al., *The glomerulo-tubular junction: a target in renal diseases.* J Pathol, 2002. **197**(1): p. 1-3.
6. Zhang, H., et al., *The impact of extracellular matrix coatings on the performance of human renal cells applied in bioartificial kidneys.* Biomaterials, 2009. **30**(15): p. 2899-911.
7. Baker, B.M. and C.S. Chen, *Deconstructing the third dimension: how 3D culture microenvironments alter cellular cues.* J Cell Sci, 2012. **125**(Pt 13): p. 3015-24.
8. Kolesky, D.B., et al., *Three-dimensional bioprinting of thick vascularized tissues.* Proc Natl Acad Sci U S A, 2016. **113**(12): p. 3179-84.
9. Homan, K.A., et al., *Bioprinting of 3D Convoluted Renal Proximal Tubules on Perfusable Chips.* Sci Rep, 2016. **6**: p. 34845.
10. Grabias, B.M. and K. Konstantopoulos, *Epithelial-mesenchymal transition and fibrosis are mutually exclusive reponses in shear-activated proximal tubular epithelial cells.* Faseb j, 2012. **26**(10): p. 4131-41.
11. Papaioannou, T.G. and C. Stefanadis, *Vascular wall shear stress: basic principles and methods.* Hellenic J Cardiol, 2005. **46**(1): p. 9-15.
12. Jang, K.J., et al., *Human kidney proximal tubule-on-a-chip for drug transport and nephrotoxicity assessment.* Integr Biol (Camb), 2013. **5**(9): p. 1119-29.
13. Sekiya, S., et al., *Hormone supplying renal cell sheet in vivo produced by tissue engineering technology.* Biores Open Access, 2013. **2**(1): p. 12-9.
14. Weber, E.J., et al., *Development of a microphysiological model of human kidney proximal tubule function.* Kidney Int, 2016. **90**(3): p. 627-37.
15. Wilmer, M.J., et al., *Kidney-on-a-Chip Technology for Drug-Induced Nephrotoxicity Screening.* Trends Biotechnol, 2016. **34**(2): p. 156-70.

16. Lee, V.K., et al., *Creating perfused functional vascular channels using 3D bio-printing technology.* Biomaterials, 2014. **35**(28): p. 8092-102.
17. King, S.M., et al., *3D Proximal Tubule Tissues Recapitulate Key Aspects of Renal Physiology to Enable Nephrotoxicity Testing.* Front Physiol, 2017. **8**: p. 123.
18. Bakker, R.C., et al., *Renal tubular epithelial cell death and cyclosporin A.* Nephrology Dialysis Transplantation, 2002. **17**(7): p. 1181-1188.
19. Lovett, M., et al., *Vascularization Strategies for Tissue Engineering.* Tissue Eng Part B Rev, 2009. **15**(3): p. 353-70.
20. Miya, M., et al., *Enhancement of in vitro human tubulogenesis by endothelial cell-derived factors: implications for in vivo tubular regeneration after injury.* Am J Physiol Renal Physiol, 2011. **301**(2): p. F387-95.